Hyperfine pumping of SrF states

Masterthesis Applied Physics

B.H.P. Drolenga BSc.

University of Groningen, Faculty of Mathematics and Natural Sciences
Van Swinderen Institute for Particle Physics and Gravity

September 29, 2014

Contents

Chapter 1

Introduction

1.1 Cold Molecules

In our research group we are decelerating heavy diatomic molecules in combination with laser cooling, in order to achieve ultracold molecules of Strontiumfluoride (SrF). Three seperate cooling states can be distinguished. First, a cold SrF molecular beam is produced using laser ablation of a SrF_2-pill. A xenon or argon gas pulse picks up the molecules, forming a supersonic molecular beam. An unique design of a Stark-decelerator is used to trap and decelerate molecules to a standstill. Finally, laser cooling is applied to reduce the temperature even further.

When the decelerated or guided molecules exit the decelerator, detection takes place using laser-induced fluorescence (LIF). The frequency of the laser is tuned to excite SrF molecules within the decelerated molecular beam, whereafter the decay path of the same transition is detected. Alternatively, off-resonant detection could be applied using, where a irreversible decay path of a different transition is measured. Details about the experimental lay-out and the energy level structure of SrF can be found in chapter 2 and 3.

Control over ultracold molecules could be highly benificial in exciting high-precision fundamental measurements and physics, like molecular clocks, quantum computing etc. In our research group we plan to measure parity violation (PV) in molecules. For atoms PV already has been measured for the first time in 1957 [1]. PV was never observed in molecules before. Recently, Barry et al. succeeded to trap SrF molecules in a 3-D magneto-optical trap (MOT) [2]. For high-precision measurements, like PV in molecules, a high number of trapped molecules is highly required. A substantial amount of molecules are lost during the deceleration in the traveling-wave Stark decelerator. In this report, the possibility to depress such losses by introducing a optical frequency laser beam before the molecules are entering the decelerator is investigated.

1.1.1 What has been done in the ColdMol group

From 2010 till now a 4 meter traveling-wave Stark decelerator is build-up at the Van Swinderen Institute for Particle Physics and Gravity (former Kernfysisch Versneller Institute (KVI)) in Groningen, Netherlands. Untill the time of this writing, we managed to detect and decelerate molecules after 2 meter from 300 m/s to 234 m/s, using a nitrogen-cooled supersonic expansion of Xenon. Results are publicated recently in [3]. Ref. [4] present results of numerical simulations showing the high stability and efficiency of heavy diatomic molecule trapping and deceleration using a traveling-wave Stark decelerator.

We plan to further extended our decelerator to 4.5 meter length. Currently, molecules can be detected in the guiding (zero deceleration) mode after 4 meter (see figure 1.1). Currently, deceleration and hyperfine pumping experiments, the main content of this thesis, are in progress. The ultimate goal is to bring the traps with molecules of the traveling-wave decelerator to a standstill and further laser cool the SrF molecules. Finally, we plan to load the molecules in a optical dipole trap, where PV will be measured.

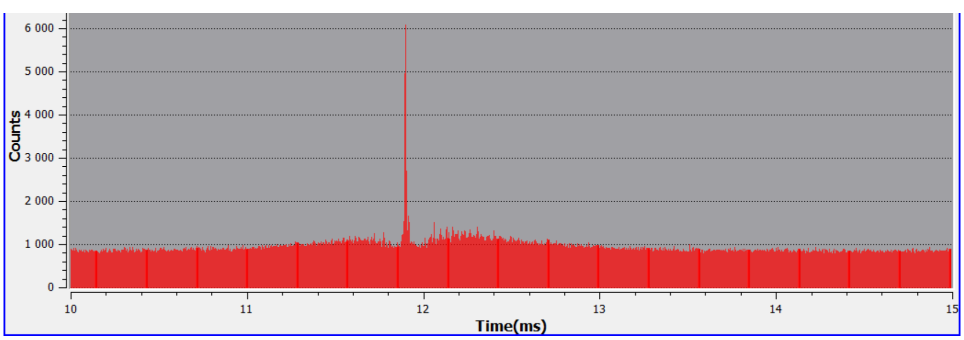

Figure 1.1: SrF signal after 4 meter of AC-guiding in the traveling-wave decelerator. The arrival time of the molecules corresponds with an initial velocity of 370 m/s of the xenon beam.

1.1.2 In this report

Possible improvements for increasing the number of molecules trapped at the end of the decelerator are investigated. Since the decelerator is designed only for the deceleration of specific SrF hyperfine states, the possibility of manipulating the hyperfine state concentration before deceleration is explored. Optical pumping at the begin of the deceleration could increase the number of trapped molecules by a factor 1.2. A laser beam which crosses the molecular beam perpendicular at the beginning of the decelerator, can influence the hyperfine state of a single molecule. The same laser system enables utilization of an additional detection system at the beginning of the decelerator. This detection systems benefits the optimization of the detection signal at the end of the decelerator. The interaction of SrF molecules with light is modelled using Multi-Level Rate Equations (MLREs), derived from the Einstein Rate Equations (EREs). The electric and magnetic field strength and the laser characeristics are varied in the simulations in order to examine the maximum gain and most appropriate parameters.

Chapter 2 describes the experimental lay-out and working principle of the Stark decelerator. Chapter 3 provides a detailed description of the interaction of SrF molecules with laser light and external fields. Chapter 4 finally explains the build-up and results of the experiment and simulations which model the optical pumping. Chapter 5 includes the appendices.

Chapter 2

Traveling wave deceleration

2.1 Experimental lay-out

The most unique and novel apparatus we use in our research, is the traveling-wave decelerator. A supersonic molecular beam propagates through a 5-meter long cylindrical-shaped decelerator consisting out of 8 modules with more than 500 ring-shaped electrodes of 4 mm diameter, 0.6 mm thickness and a center-to-center spacing of 1.5 mm.

First, the beam is created by ablating a pill of SrF_2 with a Nd:YAG laser in vacuum. A gas pulse of xenon/argon superconically expands in the source chamber, which carries the molecules out of the chamber. Currently, we are working on a gas valve which is cooled with nitrogen of -30 °C, resulting ultimately in a supersonic molecular beam with velocity 280 m/s (xenon). Uncooled beams have an average velocity of 370 m/s (xenon) or 550 m/s (argon) and a rotational temperature of 10 K [3]. A supersonic molecular beam is required for our research, to be able to decelerate and trap a large number of molecules. The molecular beam passes through a skimmer of 1 mm diameter located approximately 10 cm from the ablation spot. The skimmer makes sure that molecules which fall outside the phase-space acceptance of the decelerator are not able to build up pressure inside the vacuum chambers. The skimmed beam propagates a few centimeter before it enters the decelerator. By applying a time-varying sine wave voltage to the electrodes, a repetition of moving electric field minima and maxima are created. The formed potential wells are able to trap and decelerate SrF molecules due to the Stark shift of the molecules. After optimal deceleration (which corresponds to a standstill of the traps), molecules have a maximum velocity of 5.8 m/s corresponding to rotational temperature of 215 mK.

Laser cooling is applied to further lower the temperature ultimately to a temperature of $10 - 100\ \mu$K. At the end of the decelerator molecules can be detected using a photomultiplier (PMT). A second detection system between the ablation position and the beginning of the decelerator is build up during the research in this thesis. Figure 2.1 shows the geometry of the decelerator.

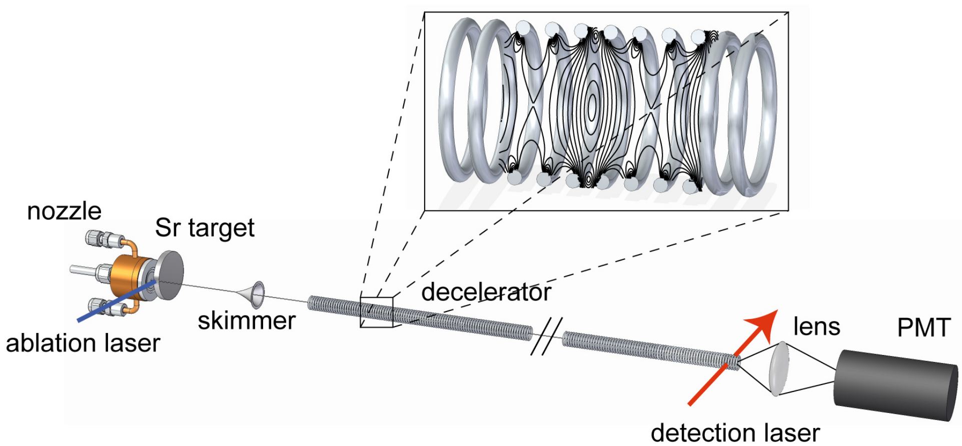

Figure 2.1: Experimental set-up. A SrF_2 pill is ablated with a laser and a supersonic molecular beam is created. After deceleration a detection laser is used to excite the molecules. The scattered light is focussed with a lens and collected with a PMT of detection efficiency 2%. The inset shows the electric field profile in within a few ring electrodes. The contour lines clearly shows the creation of electric field traps along the propagation axis of the molecules. The new detection system we are building up now is not in the figure. Figure is adapted from [3].

2.2 Stark deceleration

2.2.1 Working principle

Due to the intrinsic electric dipole moment of polar molecules, energy levels shift when an electric field is applied. Just like atoms, if a molecule experiences a nonzero magnetic and/or electric field, it undergoes a Zeeman and/or Stark shift. Figure 2.2 shows the Stark shift of SrF molecules for different (N, M)-states. N is the rotational quantum number, where M is the projection of N on the electric field axis. A negative (positive) Stark shift gradient forms a downhill (uphill) potential landscape for a molecule along the curve and determines if a molecule is high-field (low-field) seeking. It can be seen from the figure that not all states are low-field seeking. Actually, within the $(1, 0)$ curve, only 4 out of 12 hyperfine states are low-field seeking. During deceleration, the high-field seeking molecules are lost and cannot be trapped. The upper limit for the electric field strength during the operation of Stark deceleration is ~20 kV/cm, which can be seen in the Stark curve of the $(1, 0)$ state at the saddle point. All the molecular states are high-field seeking beyond this maximum electric field strength.

When molecules experience an inhomogeneous electric field, the gradient of the Stark curve $W(E)$ determines a force $F = -\nabla W(E)$ on the molecules. When a molecule propagates through an inhomogeneous electric field, it climbs up (dependent on the specific shape of the Stark curve) a potential hill and transfers kinetic into potential energy. When the molecule reaches the top of the potential hill and goes downhill again, the molecule would regain its original kinetic energy. If the electric field abrubtly is switched off when the molecule is at the top of the hill, the potential energy is zero again and the molecule effectively lost kinetic energy. In a traditional Stark decelerator, this process is repeated many times leading to decelerated molecules. However, in our traveling-wave decelerator, molecules which are attracted by low electric fields are continuously trapped in 3-D potential wells. Initially, these traps travel at the same velocity as the molecules. The traps with the trapped molecules inside can be decelerated. Two conditions have to be maintained in order to reach stable deceleration [5]:

1. The kinetic energy of the molecules relative to the trap is smaller than the depth of the potential well;

2. The deceleration force is balanced by the Stark force.

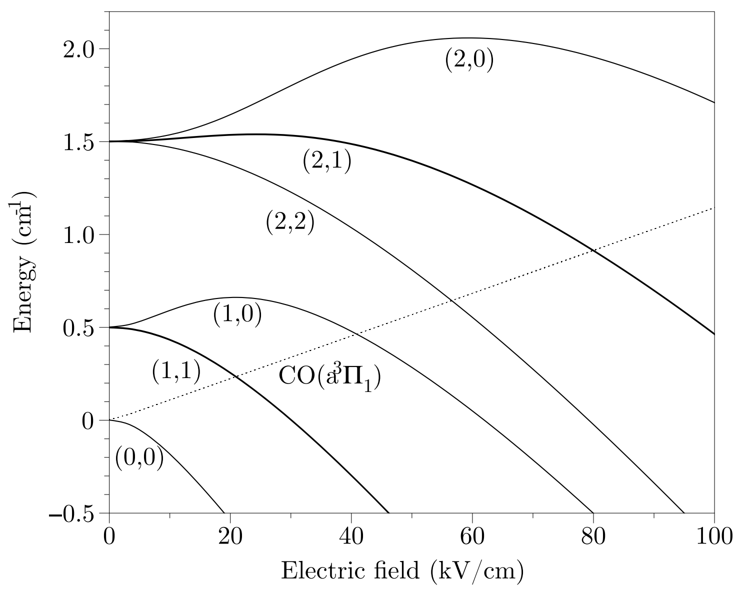

Figure 2.2: Stark shift for different (N, M)-states of SrF molecules. The $N = 1$ state is used as laser cooling and detection ground state. Only 4 of the 12 hyperfine sublevels of the $X^2\Sigma^+(v = 0, N = 1)$ state are low-field seeking. For comparison, the Stark shift of CO is shown in the figure. This Stark shift increases lineair with increasing electric field strength. The figure is taken from [4].

2.2.2 Traveling-wave deceleration

The traveling-wave decelerator creates potential traps for so-called low-field seeking molecules, i.e. molecules which are attracted to positive electric field gradients. High-field seeking molecules are attracted to high electric fields. The ring-shaped electrodes in the decelerator produce a position dependent electric field. The electrodes are connected to eight rods positioned in a octagonal pattern (see figure 2.3). An oscillating potential is applied to the n-th rod [5]:

$$V_n(t) = V_0 \cos\left(2\pi f t + 2n\pi/8\right) \tag{2.1}$$

leading to a sinusoidal potential applied on the eight consecutive electrodes. The specific waveforms applied to the electrodes, create 3D moving traps within the decelerator. Along the longitudinal direction, a repetition of electric field minima can be distinguished in the middle of the decelerator.

The inset of figure 2.1 shows an example of a steady electric field in the decelerator.

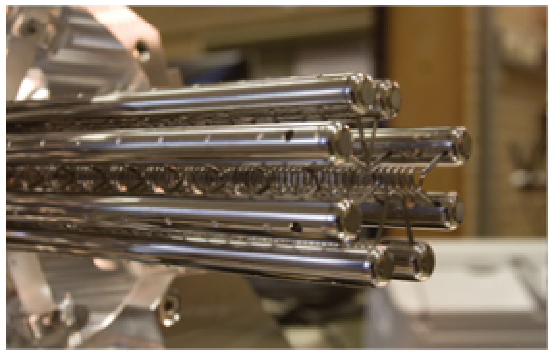

Figure 2.3: Photo of one module from the inside of the traveling-wave decelerator. The mm-sized electrodes are connected to eight octagonal oriented rods.

The main advantage of the traveling-wave decelerator is the high efficiency (high phase-space acceptance) and stability (small loss of molecules during deceleration). By changing the amplitude and the frequency of the voltage applied on the electrodes, the velocity and depth of the 3-D traps can be changed. Initially, the traps have the same velocity of the molecules. By gradually decrease the velocity of the traps by swepping down the voltage frequency, the traps and the trapped molecules are decelerated.

Due to the large mass of SrF. a relative long (5 m) decelerator is needed in order to bring a substantial amount of molecules to a standstill with modest deceleration. In contrast to SrF, light molecules like CO can be stopped within Stark-decelerators smaller than a meter. A panorama photograph of the decelerator in the lab is shown in figure 2.4.

Numerical simulations are performed to investigate the phase-space acceptance as function of the applied voltage and deceleration strength [4]. The total one-dimensional phase-space acceptance (longitudinal and transverse) is determined and compared with full 3-D simulations which include coupling between the longitudinal and transverse motion. Over 75% of the molecules inside the 1-D phase-space acceptance at the beginning of the deceleration remain trapped after 4.5 m, which make this type of Stark decelerator extremely stable and efficient. Molecules are lost when they crash at the electrodes or escape longitudinally over the potential barrier.

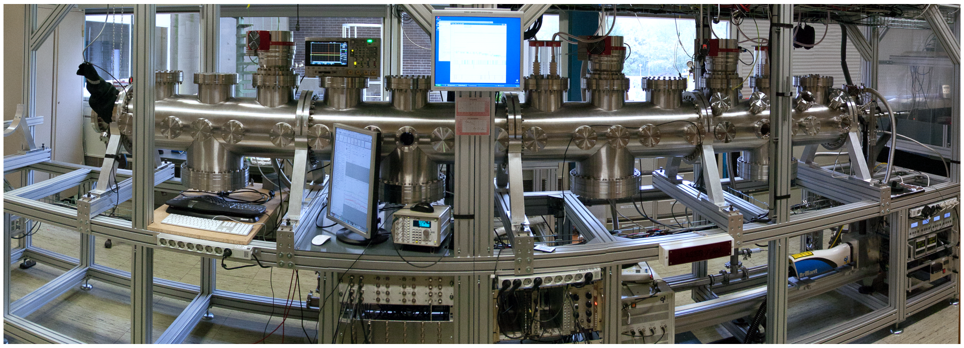

Figure 2.4: Panorama view of the decelerator in the lab. When this picture was taken the decelerator consisted out of eigth modules of 0.5 m.

2.2.3 Detection

When the decelerated or guided molecules exit the decelerator, detection takes place using laser-induced fluorescence (LIF) after 116.5 mm of free flight. The repetition rate of the measurements is 10 Hz. For example, measuring 10 minutes lead to a spectrum including 6000 shots. Destruction of the SrF-pill surface is eliminated as much as possible, by frequently changing the laser ablation spot. The initial YAG laser spot can be changed in the (x, y)-plane. Moreover, the pill is going up and down in cycles of $\sim$10 steps.

A red laser of 663 nm is generated to drive the $X^2\Sigma^+(v = 0, N = 1) \rightarrow A^2\Pi_{1/2}(v' = 0, J' = 1/2^+)$ transition, whereafter the same decay path is detected. This transition is almost closed, which makes more than one pump cycle per molecule possible. Alternatively, off-resonant detection could be applied using the $X^2\Sigma^+(v = 0, N = 1) \rightarrow A^2\Pi_{1/2}(v' = 0, J' = 1/2^+)$ decay path, using a 685 nm light filter in front of the PMT. Nevertheless, detecting this transition lead to a factor 50 decrease in signal. The main benefit of using the $X^2\Sigma^+(v = 0, N = 1) \rightarrow A^2\Pi_{1/2}(v' = 0, J' = 1/2^+)$ transition for detection, is the fact that the same laser can be used for laser cooling of SrF. More details about the energy level structure of SrF are discussed in chapter 3. The detection laser consists out of four frequency sidebands created by an electro-optical (EOM) and acoustic (AOM) modulator. The sidebands are typically $10 - 100$ MHz detuned from the central frequency to overlap the resolved hyperfine levels of the $X^2\Sigma^+(v = 0, N = 1)$ state. Details about the creation of the frequency sidebands can be found in the appendices. The detection laser crosses the molecular beam at right angle. Emitted photons from spontaneous decay are detected by a PMT after collecting and focussing of the scattered photons by a mirror and a lens as in figure 2.1.

Chapter 3

Optical pumping of SrF molecules

3.1 Energy structure of SrF molecules

3.1.1 Molecules

In contrast to atoms, molecules have a much richer internal electrical structure. Figure 3.1 shows the relevant energy levels of SrF for this research. Molecules have besides the electronic energy levels, vibrational and rotational levels due to interactions between the atomic building blocks of a molecule. Vibrational and rotational modes arise from the fact that the nuclei can vibrate along the internucleur axis and rotate around each other. The vibrational modes are labelled by v. Typical energy spacings between two vibrational levels are tens of THz. Spacings between lower rotational levels are in the order of tens of GHz. The splitting between two electronic states is in the order of $\sim$100 THz.

3.1.2 SrF structure

The spin of SrF is $S = 1/2$ and the nuclear spin is $I = 1/2$. The electronic state $X^2\Sigma^+$ is best described as a Hund's case (b) system. The electronic angular momentum L is strongly coupled to the internuclear axis forming Λ. N is formed by coupling Λ with the angular momentum of the rotating nuclei R. The rotational energy levels N split up in doublets due to spin-rotation interaction. For the electronic ground state this results in a $J = 1/2$ and $J = 3/2$ level. The hyperfine structure due to the hyperfine interaction $F = I + J$ results in a $F = 0$ and $F = 1$ level with degeneracy $g = 2F + 1$ for the $J = 1/2$ level. The hyperfine structure of $J = 3/2$ results in a three-fold $F = 1$ and a five-fold $F = 2$ level. The sublevels within a hyperfine level are labelled by $M_F = -F, -F+1, ..., F-1, F$. Energy spacings between hyperfine levels within a J-manifold are typically in the order of 50 MHz.

The first electronic excited state $A^2\Pi_{1/2}$ is best described as a Hund's case (a) system. The axial components Λ and Σ of L and S are strongly coupled due to the spin-orbit interaction, forming Ω. Since Λ and Σ can have opposite sign, Ω-doubling results in a $A^2\Pi_{1/2}$ (lowest energy) and $A^2\Pi_{3/2}$. Both states split up into two states with opposite parity due to Λ-doubling (Λ=$\pm$1 and Σ=$-1/2$). The resulting total angular momentum J is formed by the coupling between the rotation of the nuclei R and Ω. The excited state relevant for this research is $A^2\Pi_{1/2}(v' = 0, J' = 1/2^+)$. The hyperfine splitting is energetically unresolved. More details about the energy level structure of SrF can be found in [6].

After the supersonic expansion, SrF molecules are mainly populated in the rovibrational $X^2\Sigma^+(v = 0, N = 1)$ state. The decelerator is designed to decelerate molecules in some of the hyperfine levels (low-field seeking states) within this state. Moreover, the cycling transition of $X^2\Sigma^+(v = 0, N = 1) \rightarrow A^2\Pi_{1/2}(v' = 0, J' = 1/2^+)$ is almost closed which makes it highly

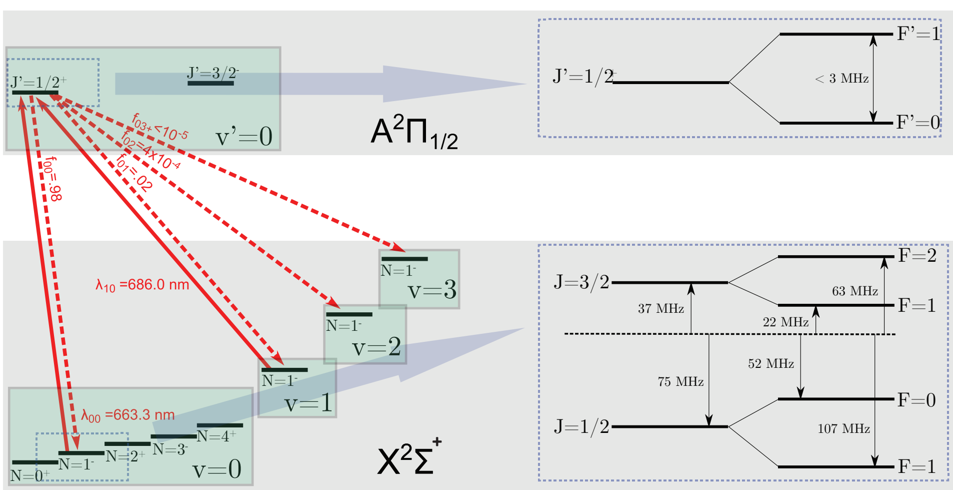

Figure 3.1: The electronic, vibrational and rotational structure of SrF. Hyperfine structure of the ground and excited state is shown on the right. The typical energy spacing between two vibrational levels are tenths of THz where the typical rotational spacing is 10 GHz. All the spacings are in angular frequency units. [8]. Part of the left figure is adapted from [7].

appropriate for laser cooling. From now, the $X^2\Sigma^+(v = 0, N = 1)$state is called the ground state and $A^2\Pi_{1/2}(v' = 0, J' = 1/2^+)$the excited state.

3.2 Optical pumping

In this section, the interaction mechanisms between SrF molecules and light will be reviewed. Optical pumping of molecules in the context of this research, is used to pump SrF molecules from high-field seeking to low-field seeking hyperfine states. The aim of this research is controlling the hyperfine population distribution (hyperfine pumping) of SrF molecules.

3.2.1 Two-level system interaction with light

Einstein formulated in 1916 three possible interaction mechanisms between light and matter. Besides photon absorption and spontaneous emission, a third process called stimulated emission can take place when an excited atom/molecule interacts with a photon, thereby creating a ground state atom/molecule and two photons. For a two-level energy system with excited state E_2 and ground state E_1, stimulated absorption, stimulated emission and spontaneous emission are governed by Einstein coefficients B_{12}, B_{21} and A_{21}. When a molecule undergoes stimulated emission, the photon is emitted in opposite direction with respect to photon absorption. Spontaneous emission or decay take place in random direction. The Einstein coefficients reflect the probability for a process to occur. The relation between B_{12} and B_{21} is:

$$\frac{B_{12}}{B_{21}} = \frac{g_1}{g_2} \tag{3.1}$$

where g_i is the degeneracy of state i. For a two-level system the degeneracy of both levels is equal (one-half); therefore $B_{12} = B_{21}$. A schematic of the absorption and emission processes for a two-level system is shown in figure 3.2.

The Einstein Rate Equations (EREs) based on these three constants, can be used to model and simulate the population in a two or multi-level system. With certain assumptions it is a simplification of the semi-classical Optical Bloch Equations (OBEs) [9] [10]. OBEs describe the dynamics of a two-level quantum system interacting with electromagnetic radiation. Coherences are neglected in the rate equation approach. At short time scales the solutions of the OBEs and EREs differ. In the limit of the steady-state solution i.e. the time-deriatives are zero, both approaches give the same solution.

The steady state (i.e. excitation rate equals the decay rate) scattering rate R_{sc} of a two-level system is given by [18]:

$$R_{sc} = \rho_{ee}\Gamma = \frac{(I/I_s)}{1 + (I/I_s) + 4(\delta/\Gamma)^2}\frac{\Gamma}{2} \tag{3.2}$$

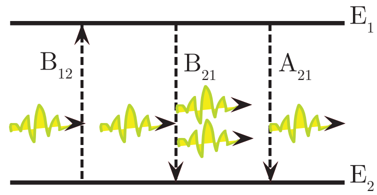

Figure 3.2: Stimulated absorption and emission governed by B_{12}. The momentum transfer involved in both processes are in opposite direction. The spontaneous decay governed by A_{21} is in random direction. The yellow wavepackets represent absorbed and emitted photons.

where ρ_{ee} is the excited state population; $s = I/I_s$ is the saturation parameter; δ is the transition detuning from resonance and Γ the natural linewidth. When $s>>1$, R_{sc} goes to $\Gamma/2$. The saturation intensity I_s for a two-level system is [18]:

$$I_s = \frac{\pi h_c \Gamma}{3\lambda^3} \tag{3.3}$$

it is defined as the intensity at which half of the maximum excited state population, physically is in the excited state.

3.2.2 SrF interaction with light

According to section 3.1, the relevant energy levels of SrF which interact with light cannot be approached as a two-level system. To scatter photons with all four hyperfine manifolds in the $X^2\Sigma^+(v = 0, N = 1)$state, four different laser frequencies have to be offered. For the multi-level system of the $X^2\Sigma^+(v = 0, N = 1) \rightarrow A^2\Pi_{1/2}(v' = 0, J' = 1/2^+)$ transition in SrF, the stimulated absorption/emission rate between a ground state i and an excited state j is [8] [14]:

$$R_{ij} = \frac{I/I_s}{1 + 4(\delta/\Gamma)^2} \frac{\Gamma}{2} \tag{3.4}$$

where the saturation intensity per laser frequency pumping hyperfine level i to excited state j is defined by:

$$I_{s(ij)} = \frac{\pi h c \Gamma}{3\lambda^3} \frac{1}{r_{ji}} \tag{3.5}$$

where r_{ji} is the branching ratio of decay from excited state j to the $N = 1$-manifold (for SrF see table 3.1 and 3.3). The spontaneous decay rate Γ_{ji}

from excited state j to ground state i is equal to [14] [8]:

$$\Gamma_{ji} = \Gamma r_{ji} \tag{3.6}$$

The overall scattering rate R_{sc} for a multi-level system is defined is:

$$R_{sc} = \Gamma \rho_e \tag{3.7}$$

where ρ_e is the total excited state population. When there is steady state pumping, i.e. there are no decay paths (subsection 3.2.3) or dark states (subsection 3.3.1), the overall scattering rate R for SrF can be approximated as (according to interpolation of the overall scattering rate for a two-level system and the diatomic molecule YbF [16]):

$$R = \frac{I/(2I_s)}{1 + I/(2I_s) + 4(\delta/\Gamma)^2} \frac{\Gamma}{4} \tag{3.8}$$

When $I = 2I_s$ and $\delta = 0$ for SrF this corresponds to 5.2 MHz. Note that the saturation intensity I_s is referred to the overall saturation intensity of the $X^2\Sigma^+(v = 0, N = 1) \rightarrow A^2\Pi_{1/2}(v' = 0, J' = 1/2^+)$ transition (= 3.0 mW/cm^2), and not to the saturation intensity of a specific transition between ground state i and excited state j in the $X^2\Sigma^+(v = 0, N = 1) \rightarrow A^2\Pi_{1/2}(v' = 0, J' = 1/2^+)$transition. At complete saturation (i.e. $I >> I_s$), this expression reduces to [17]:

$$R_{max} = \Gamma \frac{N_e}{N_e + N_g} \tag{3.9}$$

where N_e and N_g are the number of excited and ground state sublevels. For SrF R_{max} corresponds to 10.4 MHz.

3.2.3 Branching ratio's and selection rules

The probability of a decay transition between two arbitrary vibrational electronic levels to occur, are described by the Franck-Condon factors (FCFs). FCFs describe the overlap between the wavefunctions of two vibrational states. The vibrational branching ratio's (VBRs) depend besides the FCFs on the energy difference between the transition. Table 3.1 shows a few relevant VBRs for the $X^2\Sigma^+ \rightarrow A^2\Pi_{1/2}$ transition. The procedure for calculating the FCFs and VBRs can be found in [8]. Allowed electric dipole transitions between a $X^2\Sigma^+(v = 0, N = 1)$ and $A^2\Pi_{1/2}(v' = 0, J' = 1/2^+)$ sublevel are governed by the following selection rules:

$$\pi_F = -\pi_i \tag{3.10}$$

$$\Delta F = 0, \pm 1 \tag{3.11}$$

$$\Delta M_F = 0, \pm 1 \tag{3.12}$$

One exception on selection rule 3.11 and 3.12: if $F = 0 \rightarrow \Delta F \neq 0$ and if $M_F = 0 \rightarrow \Delta M_F \neq 0$. Equation 3.10 forbids transitions between states of the same parity. The branching ratio of a transition between two levels describes the distribution of intensity over the various rotational, spin-rotational and hyperfine levels involved. Table 3.2 shows some branching ratio's between the lowest $X^2\Sigma^+ \rightarrow A^2\Pi_{1/2}$ transitions. As can be seen in this table, dipole transition between states of the same parity are forbidden due to the parity selection rule (3.10). In this research, the optical pumping concentrates on the $X^2\Sigma^+(v = 0, N = 1) \rightarrow A^2\Pi_{1/2}(v' = 0, J' = 1/2^+)$ transition. Note that from table 3.2 and table 3.1 it can be seen that this transition is rotational totally (branching ratio 1) and vibrational (branching ratio $\sim$0.02) almost closed. By choosing a ground state with $R = 1$ and an excited state with $R' = 0$, rotational branching is eliminated due to the parity and angular momentum selection rules, which make such a system extremely attractive for laser cooling molecules [19]. Table 3.3 shows the BRs of decay between all rotational, spin-rotational and hyperfine levels involved within the $X^2\Sigma^+(v = 0, N = 1) \rightarrow A^2\Pi_{1/2}(v' = 0, J' = 1/2^+)$ transition.

FCFs	$v" = 0$	$v" = 1$	$v" = 2$
$v' = 0$	9.832e-1	1.641e-2	3.561e-4
$v' = 1$	2.046e-2	9.467e-1	3.179e-2
$v' = 2$	3.294e-5	4.048e-2	9.114e-1

Table 3.1: Some relevant VBRs for the $X^2\Sigma^+ \rightarrow A^2\Pi_{1/2}$ transition of SrF. The VBRs represent the probability for a certain transition to occur. Table adapted from [8].

	$N" = 0$	$N" = 1$	$N" = 2$	$N" = 3$
$J' = 1/2^+$		1		
$J' = 3/2^+$		7/10		3/10
$J' = 1/2^-$	1/3		2/3	
$J' = 3/2^-$	1/6		5/6	

Table 3.2: Branching ratio's of some of the lowest $X^2\Sigma^+ \rightarrow A^2\Pi_{1/2}$ decay paths. Table adapted from [8].

			$F' = 0$	$F' = 1$		
$J"$	$F"$	$M_F"$	$M_F' = 0$	$M_F' = -1$	$M_F' = 0$	$M_F' = 1$
3/2	2	-2	0	0.1667	0	0
		-1	0	0.0833	0.0833	0
		0	0	0.0278	0.1111	0.0278
		1	0	0	0.0833	0.0833
		2	0	0	0	0.1667
3/2	1	-1	0.0063	0.1330	0.1330	0
		0	0.0063	0.1330	0	0.1330
		1	0.0063	0	0.1330	0.1330
1/2	0	0	0	0.2222	0.2222	0.2222
1/2	1	-1	0.3271	0.1170	0.1170	0
		0	0.3271	0.1170	0	0.1170
		1	0.3271	0	0.1170	0.1170

Table 3.3: Branching ratio's between the rotational, spin-rotational and hyperfine levels of the $X^2\Sigma^+(v = 0, N = 1) \rightarrow A^2\Pi_{1/2}(v' = 0, J' = 1/2^+)$ decay paths. Table adapted from [8].

3.3 Optical cycling scheme and rate equations

The OBEs are basically the equations of motion for elements in the density matrix. The diagonal terms of the density matrix describes the probability to be in the lower of higher state. The off-diagonal terms describes the coherences of the system, i.e. the probability to be in a superposition of both states. The laser light is treated as electromagnetic radiation with an amplitude and a phase. An exact solution of the population dynamics of the system would require solving the OBEs, which lead to a system of N^2 equations and variables [8] (N is the number of states involved). Alternatively, in the limit of one of the following two approximations [10]:

1. Broadband excitation i.e. the spectral width of the light field is much greater than the the transition linewidth;

2. The relaxation rates of the relevant atomic coherences are much larger than those of the i.e. the coherence lifetime is much smaller than the population lifetimes;

the EREs approach for modelling the state population, is a valid approximation. In contrast to the OBEs, the EREs only depend on the intensity of the laser light. EREs always give the correct values for the population distribution in the steady state [10]. The EREs for a multi-level system are called Multi-Level Rate Equations (MLREs).

The population in a $X^2\Sigma^+(v = 0, N = 1)$ sublevel increases due to spontaneous and stimulated emission of a molecule occupying a $A^2\Pi_{1/2}(v' = 0, J' = 1/2^+)$ sublevel, governed by the Einstein coefficients. The population decreases due to excitation of a molecule in a $X^2\Sigma^+(v = 0, N = 1)$ sublevel to a $A^2\Pi_{1/2}(v' = 0, J' = 1/2^+)$ sublevel. The population in a $A^2\Pi_{1/2}(v' = 0, J' = 1/2^+)$ sublevel is determined in the same way with the additional decay path to a $v" > 0$ state. Without repump lasers (lasers which are able to pump 'lost' molecules from $v > 0$ sublevels back to a $A^2\Pi_{1/2}(v' = 0, J' = 1/2^+)$ sublevel) this decay is irreversible. However, for laser cooling SrF repump lasers are required in order to achieve a high number of scattered photons. The MLREs for the ground and excited state are:

$$\frac{dN_i}{dt} = \sum \Gamma_{ij} N_j - \sum R_{ij}(N_i - N_j) \tag{3.13}$$

$$\frac{dN_j}{dt} = -\sum \Gamma_{ij} N_j + \sum R_{ij}(N_i - N_j) - VBR_{(v">0)} N_j \tag{3.14}$$

where N_i and N_j are the ground/excited state populations. R_{ij} and Γ_{ij} represent the absorption and emission rate between excited state level j and ground state level i, and are specified in subsection 3.2.2. Besides the 12 ground state and 4 excited state sublevels involved in the $X^2\Sigma^+(v = 0, N = 1) \rightarrow A^2\Pi_{1/2}(v' = 0, J' = 1/2^+)$ transition (figure 4.1), vibrational and rotational branching leads to population in higher vibrational and rotational states. However, for the cycling transition which is used in this research, rotational branching is not important (branching ratio$< 10^{-6}$, see table 3.2). Vibrational branching to $(v" > 0) = \sim 0.02$ (see table 3.1) cannot be neglected at modest number of pump cycles when modelling the state populations. The factor $VBR_{(v">0)}$ accounts for this and is the vibrational branching ratio (can be found in table 3.1). Nevertheless, the diagonal FCFs, which partly determine the probability of a $v' \neq v"$ transition, are relatively suppressed for SrF. This makes SrF a good candidate for optical pumping and laser cooling.

For lineair polarized light, which we use in this experiment, equation 3.15 allows electric dipole transitions only if the states involved have the same magnetic quantum number M_F. This reduces 3.12 to:

$$\Delta M_F = 0 \tag{3.15}$$

For SrF this implies that in the $X^2\Sigma^+(v = 0, N = 1) \rightarrow A^2\Pi_{1/2}(v' = 0, J' = 1/2^+)$ transition the $J = 3/2$ $(F, M_F) = (2, \pm 2)$ cannot be excited. These states are called *dark states*. Due to the presence of dark states and the nonzero vibrational decay in our system, the overall scattering rate will be lower compared to the estimations of section 3.2.2.

3.3.1 Magnetic field remixing

A small magnetic field of a few Gauss can be applied to repopulate the sublevels within a hyperfine manifold [12]. The magnetic field will cause Larmor precession of the magnetic sublevels. Within a hyperfine manifold, the magnetic sublevels will mix when $\Delta M_F = \pm 1$. The remixing rate will be [8] [16]:

$$\Gamma_{remix} = \frac{g_F \mu_B B}{h} \tag{3.16}$$

where $\mu_B = 9.274 \times 10^{-24}$ is the Bohr magneton, B the magnetic field strength (typically a few Gauss), g_F the g-factor of the relevant F-manifold and $h = 6.626 \times 10^{-34}$ is Planck's constant. The g-factors of the $X^2\Sigma^+(v = 0, N = 1)$ state are $-0.33, 0, 0.83$ and 0.50 for $(J, F) = (\frac{1}{2}, 1), (\frac{1}{2}, 0), (\frac{3}{2}, 1)$

and $(\frac{3}{2}, 2)$ [8]. The magnetic field cannot be too large, since it induces Zeeman shifts of the magnetic sublevels which could bring transitions out of resonance. The Zeeman shift of a magnetic sublevel is equal to:

$$\Delta E = \frac{\mu_B B g_F M_F}{\hbar} \tag{3.17}$$

Remixing adds an extra term to rate equation 3.13:

$$\sum \Gamma_{remix,ik}(N_i - N_k) \tag{3.18}$$

where the sum for sublevel i runs over the sublevels k with $\Delta M_F = \pm 1$ within the same F-manifold. The remixing of the excited state sublevels is neglected since these g-factors are almost zero.

3.4 Laser cooling

When the traveling-wave traps in the Stark decelerator brought to standstill, further laser cooling is applied in order to decrease the temperature of the trap in the $10-100\mu$K regime. Since the formulation of quantum mechanics in the beginning of the 20th century, people agree about that waves, like masless photons, have momentum and are able to transfer it. Laser cooling works due to the momentum transfer of light.

Consider the two-level system of figure 3.2. If an atomic or molecular beam with this closed cycling transition is propagating for example in the x-direction, a laser with frequency $\nu = E_2 - E_1$ coming from the $-x$-direction pumps the incoming particles back and forth between E_1 and E_2. Since the process of spontaneous emission is in random direction, stimulated absorption and emission result in a net force in the $-x$-direction. In this way the particle beam can be decelerated longitudinal or transversely deflected. A 3-D system of six resonant laser beams in $\pm x, \pm y$, and $\pm z$ is in this way able to trap and cool particles inside the interaction zones of the laser. A magneto-optical trap (MOT) can be produced when these six laser beams are combined with a spatial dependent magnetic field, leading ultimately to ultracold temperatures even below the Doppler limit.

In order to reach low temperatures with laser cooling, two important prerequisites are:

1. (Almost) closed transition;

2. High spontaneous decay rate i.e. short lifetime.

An almost closed transition is required so that a lot of cycles can take place before a molecule decay to a seperate dark state. For a two-level system the transition is closed, obviously. A high spontaneous decay rate is necessary since the interaction time for laser cooling or slowing of a molecular beam is typically in the $1-100\mu$s-regime. The spontaneous decay rate or spontaneous scattering rate Γ is inversely proportional to the lifetime τ: $\Gamma = \frac{1}{\tau}$. For a two-level system the overall scattering rate cannot exceed $\frac{\Gamma}{2}$, since in the extreme case the particle spend equal time in the ground and excited state. For a multi-level system, like the SrF energy scheme from subsection 3.2.2, the maximum scattering rate can be approximated by [16]:

$$R_{scatt,max} = \frac{\#\text{ excited state sublevels}}{\#\text{ total sublevels}}\Gamma \tag{3.19}$$

Under the assumption that all transitions involved are excited. For the $X^2\Sigma^+(v = 0, N = 1) \rightarrow A^2\Pi_{1/2}(v' = 0, J' = 1/2^+)$ transition in SrF, neglecting vibrational leaking and dark state manifestation, this corresponds to a maximum scattering rate of $\frac{4}{4+12}\Gamma = \frac{\Gamma}{4} = 10.4$ MHz.

Chapter 4

Hyperfine pumping simulations

A high number of trapped molecules is a key factor for the parity violation measurements our research group is planning to do. Currently, our research group is investigating the possibility to improve the source chamber and laser ablation of the SrF_2 pill design, leading to more SrF molecules per ablation laser pulse.

During deceleration, molecules are lost due to several processes. The main obstacle is the existence of high-field seeking molecules. These molecules are deflected instead of attracted by low electric field, and crash at the decelerator walls. A laser with frequencies addressing the high-field seeking hyperfine levels of the $X^2\Sigma^+(v = 0, N = 1)$ state shines through the molecular beam 10 cm after the begin of the decelerator. This laser pumps molecules which are in the high-field seeking state to a low-field seeking state irreversibily. A schematic can be found in figure 4.5.

In order to know if optical pumping before the deceleration starts brings significant gain in number of trapped molecules, simulations has been done using MATLAB. MLREs are used to describe the interaction of molecules with laser light. These equations are solved using the *ordinary differential equation solver* (`ode15s`) in MATLAB. In the first section, the results with and without electric fied are shown which investigate the approximate potential gain dynamics. In the second part these details and the corresponding effects on the outcome of the simulations are discussed. Finally, possible improvements and errors in the codes are discussed. Currently, measurements with optical hyperfine pumping are being prepared.

4.1 Potential gain in low-field seeking molecules

4.1.1 Optical cycling scheme

The transition we use for the hyperfine pumping is the $X^2\Sigma^+(v=0, N=1) \rightarrow A^2\Pi_{1/2}(v'=0, J'=1/2^+)$ transition (see figure 3.1). After the ablation of the SrF_2 pill, the molecules are assumed to be equally distributed over all 12 hyperfine levels of the ground state. 4 hyperfine levels (4/12 of the population) are low-field seeking. The other molecules (8/12 of the population) are high-field seeking and therefore cannot be trapped at all and are always lost. The maximum number of molecules which can be trapped and laser cooled in the end is thus limited by the low-field seeking state concentration. The hyperfine structure including the magnetic sublevels of the ground and excited state is shown in figure 4.1. If molecules in the $(J, F) = (1/2, 1)$ and/or $(1/2, 0)$ manifolds of the ground state are optically pumped to the excited state, they spontaneuosly decay back to the ground state substates with probabilities governed by the branching ratio's from table 3.3. These hyperfine manifolds can be addressed by making two sidebands in the frequency spectrum of the laser (see appendices). When molecules ultimately arrive in the $(J, F) = (3/2, 1)$, $(3/2, 2)$ dark states, they do not 'see' the laser anymore since the pump transition is too far detuned from resonance with respect to the laser spectrum. In this sense, the concentration in the low-field seeking states can be improved, since the are mostly pumped away to the partly low-field seeking dark states. A minority of the molecules will decay to higher vibrational states with $v" > 0$. It is worthy noting that the number and the intensity of the sidebands can be easily changed.

4.1.2 Limitations

Vibrational decay

It is not possible to pump all the molecules directly to the $J = 3/2$ hyperfine manifolds. A minor loss mechanism why this limit cannot be reached is the vibrational decay. The probability for a molecule decaying to the higher vibrational states $X^2\Sigma^+(v" > 0, N" = 1)$ is $\sim$0.02 (table 3.1). A repump laser adressing the $X^2\Sigma^+(v=0, N=1) \rightarrow A^2\Pi_{1/2}(v'=0, J'=1/2^+)$ transition could be used to pump molecules back into the cycling transition. However, after $\sim$4 pumping cycles more than 50% of all molecules are in $(J, F) = (3/2, 1)$ or $(3/2, 2)$ dark states, so this loss is negligible.

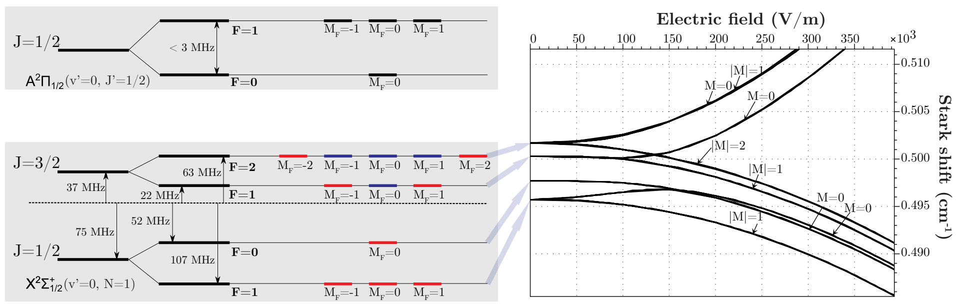

Figure 4.1: Hyperfine structure of the ground and excited state. The ground state levels $(F, M_F) = (1,0), (2,-1), (2,0)$ and $(2,1)$ of $J = 3/2$ are low-field seeking (blue levels). The other magnetic sublevels of the ground state are high-field seeking (red levels). The excited state sublevels are all low-field seeking. The hyperfine splitting in the ground state is typically $10 - 100$ MHz, where the excited state is energytically unresolved.

Dark states

A second loss mechanism is a nonzero probability for decay to high-field seeking instead of low-field seeking states, within the dark state manifolds (see branching ratio's in chapter 3). If the probability of decay to a high-field seeking dark state is higher than decay to the low-field seeking dark state, the application of a small magnetic field of a few Gauss would lead to uniform repopulation of the magnetic substates within all the F-manifolds [12]. In this case the total population would be equal devided over the low-field and high-field seeking dark states. This issue is further discussed in this chapter.

Laser characteristics

Possible losses could arise from unfavorable laser characteristics. Intense laser beams lead to high scattering rates, but induce unwanted off-resonant excitation of the dark states due to power broadening. If the laser is intense enough, dark states can be excited despite substantial detuning. If the low-field seeking dark states are pumped away and ultimately end up in the high-field seeking dark states, again a magnetic field can be used to remix these states. On the other hand, weak laser beams result in modest scattering rates. The interaction time can be increased to reach population saturation (steady state). This can be accomplished by increasing the spot width of the laser beam. On the other hand, when operating at maximum laser power, a larger laser spot area results in lower intensity again. Obviously, a trade-off between intensity and laser spot area has to be made, in order to achieve maximum gain in low-field seeking molecules. The laser sideband spectrum resolution is limited by some level ($0.1-1$ MHz). Small distortions at unwanted frequencies between the 'target' (resonance) frequencies can influence the pumping at some level.

Electric field

The limitations of the potential gain of the optical pumping when the electric field is switched on, could be due to the initial position of the molecules in a trap. A high-field seeking molecule which is initially close to electrodes, is more likely to crash instead of a undeflected molecule traveling along the beam axis. Moreover, since the Stark shift is position dependent, the transition wavelength for every molecule is different due to the position-dependent Stark shift. A possible solution could be a short switch-off of the electric field when the molecules are passing through the laser beam. In contrast, leaving the electric field switched on could have the benifit that at modest electric fields the low-field and high-field seeking states are energytically more resolved (figure 4.1).

4.1.3 Simplifications

When the molecules leave the gas valve in the supersonic expansion, they propagate 10 cm of free-flight inside the source chamber before crossing a skimmer with 2 mm diameter, which act as a blocking wall for molecules who fall outside the acceptance of the decelerator. In this way unusable molecules do not enter the decelerator and are not able to build up pressure in the decelerator chambers. It is assumed that molecules have a uniform transverse spatial distribution when they enter the decelerator (figure 4.2). When the molecules have propagated another ~10 cm inside the decelerator, they cross the excitation laser which is perpendicular on the beam axis. Initially, the molecules have a gaussian-shaped transverse velocity v_{trans} with $\mu = 0$ m/s and $\sigma = 30$ m/s. The longitudinal velocity v_z is ~370 m/s (for xenon as carrier gas) and assumed to be constant for all molecules. The molecules are spatially uniform distributed over the valve area with 1 mm diameter. In the transverse spatial distribution 20 cm after ablation, which is shown in figure 4.2b, it can be clearly seen that at the pump laser ()i.e. the laser which excites the molecules) position the molecules have approximate a uniform transverse spatial distribution.

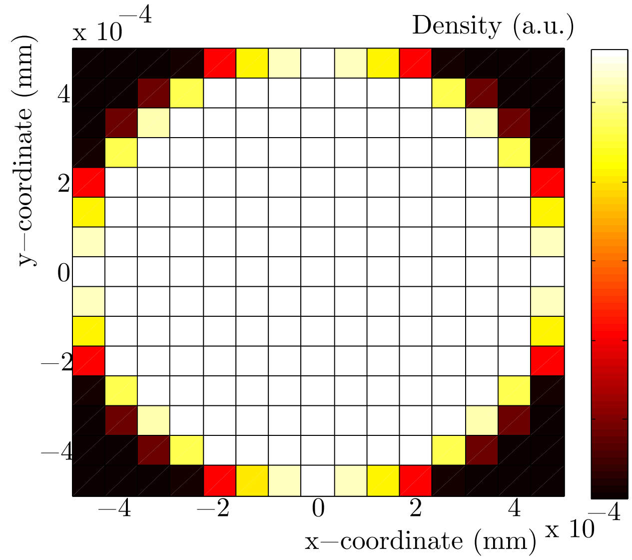

(a) Transverse spatial distribution of molecules over the gas valve area.

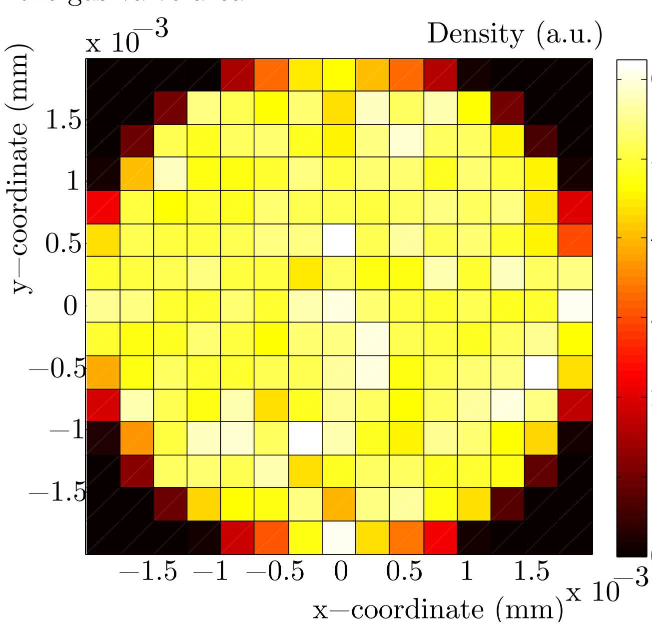

(b) Transverse spatial distribution of molecules over the decelerator cross section. Clearly, a uniform distribution can be assumed.

Figure 4.2: These plots show the spatial density of SrF molecules for (a) the initial position (at the gas valve) and (b) at the pump laser position. The trajectory of $1{\times}10^8$ molecules is simulated where a 1 mm skimmar placed after 10 cm of propagation. Most molecules fall outside the acceptance of the skimmer.

The initial transverse position of a molecule crossing the laser is assumed to remain constant during the propagation when crossing the laser beam, since transverse deflection of the molecular beam becomes significant after scattering many photons. A individual molecule undergoes ∼4 absorption cycles on average before ending up in a dark state. The corresponding change in velocity due to 4 absorption cycles is $\Delta v = 4 \times \frac{hk}{2\pi m} = 40 \times \frac{h}{\lambda m} = 22.4$ mm/s. When the laser beam has a width of 5 mm, the interaction time t_{int} and corresponding maximum transverse deflection s_{defl} would be:

$$t_{int} = \frac{5 \text{ mm}}{370 \text{ m/s}} = 13.5\ \mu\text{s} \tag{4.1}$$

$$s_{defl} = 22.4 \text{ mm/s} \times 13.5\ \mu\text{s} = 302 \text{ nm} \tag{4.2}$$

At the position of the pump laser it is assumed that the molecules have zero transverse initial velocity due to the guiding/trapping effect of the electric field.

Decay to electronic ground states with $N" \neq 1$ or $v" > 1$ is neglected since these probabilities are small ($<10^{-3}$). Branching ratio's are shown in tables 3.1, 3.2 and 3.3. Repump laser are not required, since the probability for a molecule to end up in a bright state, i.e. a state in which a molecule can be excited, after aproximately 4 pumping cycles already is $(\frac{10}{12}^4)<50\%$ where the probability for vibrational leaking is no more than 2%.

Deceleration of the traps can be neglected, since the interaction length is small compared to the change in interaction time with and without deceleration. When the laser beam again has a width of 5 mm and the deceleration strength is 9000 m/s (corresponding to the deceleration strength needed to stop molecules of $v_z = 300$ m/s (cooled valve) with a 5 m decelerator):

$$s_{int} = \frac{1}{2}at'^2_{int} + v_z t'_{int} \tag{4.3}$$

which lead to an interaction time $t'_{int} = 13.514\ \mu$s with deceleration. Compared to $t_{int} = 13.511\ \mu$s without deceleration this difference is obviously negligible.

The design of the decelerator enables a flexible way of controlling the electric fields. For example, by gradually increasing the voltage applied to the electrodes, the direct load on the high-voltage amplifiers is expected to be lower. If the presence of an nonzero electric field is an obstacle for hyperfine pumping, the electric could be switched off when the molecules cross the excitation laser. Therefore, the hyperfine pumping simulations are done for both zero and nonzero electric field.

The intensity profile of the pump laser beam is assumed to be stepfunction-like. In reality, the intensity profile follows a gaussian intensity distribution. The transverse length of the laser spot is assumed to be equal to the diameter of the electrodes. This means that all molecules which propagate through the traveling-wave decelerator, will cross the pump laser.

When the electric field and corresponding Stark shift is included in the simulation, it is important to note that only the high-field and low-field seeking Stark shift is used, i.e. see figure 2.2. The differences in Stark shift between hyperfine sublevels themself as in figure 3.1 is not included in the simulations.

4.1.4 Programming and MLREs

The backbone of the simulations is solving the MLREs described in section 3.3. The function `srf.m` simulates the MLREs which describe the interaction of a SrF molecule with light, with or without electric field. The MATLAB codes can be found in the appendices. These functions are solved using the `ode15s` solver from MATLAB. A short description of the simulations done in MATLAB is shown in MATLAB code 1. When a molecule enters the light field the simulation starts. The MLREs are solved for the longitudinal z-coordinate. The velocity of the molecules is the same as the initial velocity v_z of the supersonic expansion. In this way, the z-coordinate is easily related to the interaction time t_{int} by:

$$t_{int} = \frac{s_{int}}{v_z} \tag{4.4}$$

The simulation ends when the molecule is leaving the light field. The gain in low-field seeking molecules after passing the light field is then simply calculated by:

$$\text{Gain} = \frac{C_f - C_i}{C_i} \times 100\% \tag{4.5}$$

where C_f and C_i are the final and initial concentrations of low-field seeking molecules. The simulations are build up in the following way:

1. Initialize the **electric field profile** inside the decelerator;

2. The **molecule distribution** is assumed to be uniform in a trap when nonzero oscillating voltages are applied on the electrodes. Inside a single trap 100 random grid points are defined. One grid point represents a molecule at a specific position in the trap with electric field strength and corresponding Stark shift at that location. For zero electric field

Matlab code 1 Description of simulation codes.

```
Define parameters and constants
Define simulation parameters

if electric field is nonzero
    Define 100 grid points in a single trap
elseif electric field is zero
    Define 1 grid point in a single trap
end

for one set of simulation parameter
    Define initial concentration of sublevels
    for all grid points
        load the corresponding stark shift and detuning
        for timesteps within interaction region
            solve rate equations
        end
        save the gain of this grid point
    end
    save the average the gain over all grid points
end

plot the gain as function of the simulation parameters
```

one grid point is sufficient due to the transverse spatial independency of the simulation when the electric field is switched off;

3. Two **parameter vectors** are defined corresponding to the range of intensities and widths of the excitation laser for which the simulation is run;

4. For each laser intensity and laser width (or interaction length) the **MLRE** are simulated for all 100 grid points;

5. For **each grid point** the **gain** in low-field seeking molecules is determined;

6. Finally, **the gain in low-field seeking molecules** for a given intensity and interaction length is determined by the average of 100 grid points (or 1 grid point for zero electric field).

4.1.5 Input parameters

The longitudinal velocity at the position of the laser is equal to the longitudinal velocity v_z of the supersonic expansion with xenon or argon gas (370 or 560 m/s), since the molecules are at the very beginning of the decelerator. The other inputs are: the excited state ($A^2\Pi_{1/2}(v' = 0, J' = 1/2^+)$) natural linewidth $\Gamma = 41.7$ MHz (lifetime is 24.1 ns), saturation intensity $\mathrm{I}_s = 3.0\ \mathrm{mW/m}^2$ (procedure for determining I_s can be found in [14]) and vibrational branching ratio 0.9832.

Electric field

When the electric field in de decelerator is included in the simulation, the resulting Stark shift begins to play a role in the laser interaction with the molecules. Five different configurations of voltage waveforms can be applied on the electrodes. Distribution 1 is a cosine wave with a periodicity over eight consecutive electrodes (1-2-3-4-5-6-7-8). Distribution 2 is a cosine with a periodicity over four consecutive electrodes (1-2-3-4-1-2-3-4). Distribution 3 is a saw-tooth voltage, distribution 4 is comparable to distribution 2 but with a different periodicity (1-1-2-2-3-3-4-4), and distribution 5 corresponds to DC-guiding (+-+-+-+-). Distribution 5 creates a static guiding channel, which only confines molecules transversely but not longitudinally. The resulting Stark shift profiles due to the electric field distributions for low-field seeking ground state molecules are shown in figure 4.3.

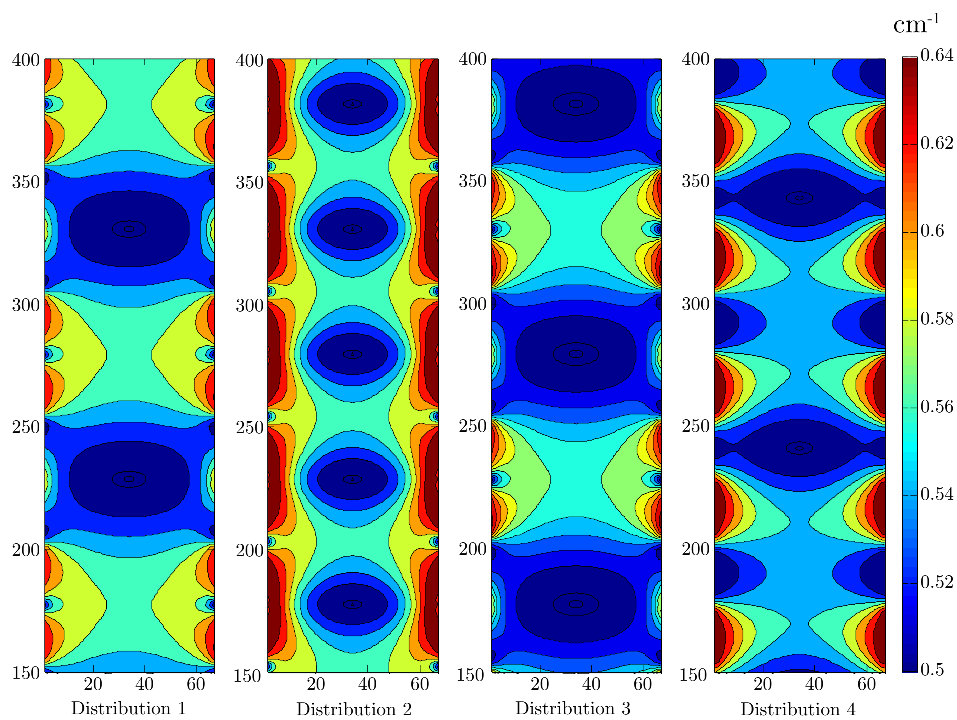

Figure 4.3: Stark shift of the low-field seeking ground state molecules for different voltage configurations. Distribution 5 is not shown. The voltage amplitude is 2.5 kV. The x and y axis of the plots represent the longitudinal and transverse position in the decelerator in arbitrary units.

In this report we only focus on distribution 1. The phase-space acceptance for this configuration is the highest [4]. Currently, our research group is investigating the possibility of using so-called 'strange waveforms', which would enable higher phase-space acceptance. The position dependent Stark shift (see figure 2.2) results in an nonzero detuning of the molecules with the laser and influences the excitation rate (equation 3.4). In the middle of the traps the electric field and stark shift are zero. The amplitude of the applied voltage determines the depth or height of the traps. The frequency of the applied voltage determines the deceleration of the traps, but in these simulations the frequency is constant during the time-of-flight and is set to a value which matches the initial velocity of the traps, i.e. guiding of the molecules.

A Monte-Carlo simulation based on individual molecules is not necessary since a uniform distribution of the molecules is assumed (see section 4.1.3). The only position-dependent parameter in the simulation is the Stark shift. 100 random points, with their corresponding Stark shift, are generated within a single trap. The program which defines these points `Stark_shift_distr_1_calculate_sp.m`, where 'sp' stands for sample points, can be found in the appendices. The Stark shift of the relevant states within a single trap is shown in figure 4.4. It is worth noting that the effective Stark shift of a state is the difference between the excited state and the ground state Stark shift. The low-field and high-field seeking excited state corresponds to the $J' = 1/2^+$ and $J' = 1/2^-$ manifolds. In this research only the $J' = 1/2^+$ excited state manifold is included in the cycling scheme. The program `srf_model_e_field.m` (see appendices) is solved for variable intensity and interaction length, for the 100 grid points. Per given intensity and interaction length, the gain in low-field seeking molecules of all the grid points is summed and devided by the number of grid points. This procedure is repeated for varying electric field strengths (i.e. trap depths).

4.1.6 Simulation parameters

The domain of interaction length L in the simulations i.e. the width of the laser beam is $0-3$ cm which corresponds to a maximum interaction time of $\tau_{int} = \frac{L_{max}}{v_z} = \frac{0.03}{370} = 81.1$ μs, assuming a stepfunction-like intensity profile. The domain of saturation parameters s in the simulations is $0 - 0.5$ I/I_S. This is *equally* divided over the number of sidebands.

The laser wavelength is 663 nm which drives the $X^2\Sigma^+(v = 0, N = 1) \rightarrow A^2\Pi_{1/2}(v' = 0, J' = 1/2^+)$ transition. The hyperfine frequency sidebands are generated around the main $X^2\Sigma^+(v = 0, N = 1) \rightarrow A^2\Pi_{1/2}(v' = 0, J' =$

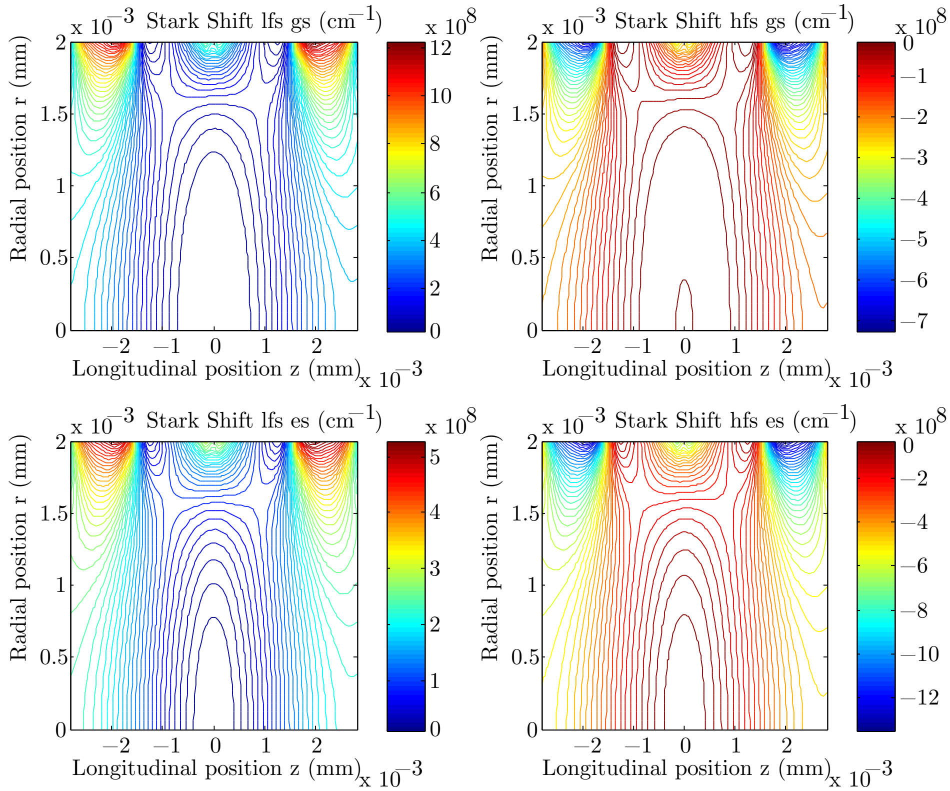

Figure 4.4: Stark shift for single traps in the distribution 1 waveform voltage configuration, with 1 kV potential applied to the electrodes. The graph shows the Stark shift for the low-field (LFS) and high-field (HFS) (left to right) seeking ground (GS) and excited (ES) states (top to bottom).

$1/2^+$) transition. Only the two most left or one most left sideband(s) are/is generated, adressing the $(J, F) = (1/2, 1)$ and $(1/2, 0)$ (see (2) of figure 4.5), which are high-field seeking. In this way the molecules from these levels are pumped to the $J = 3/2$ hyperfine levels. Distortions within the laser spectrum are not included. The shape and height of the sideband peaks are all the same for the four sidebands. For example, when using 4 sidebands in the simulation, the total laser intensity is equally divided over the sidebands.

A repump laser is not required due to favorable Franck-Condon factors. Moreover, the Stark curve for $v = 1$ molecules in the $X^2\Sigma^+(v = 0, N = 1)$ state is similar to the $v = 0$ Stark curve. These low-field seeking molecules in the $v = 1$ vibrational level are decelerated together with the

$v = 0$ molecule, and can be pumped back into the cycling scheme when laser cooling is applied with repump lasers. The geometry of the experiment and the laser illumination is shown in of figure 4.5(a).

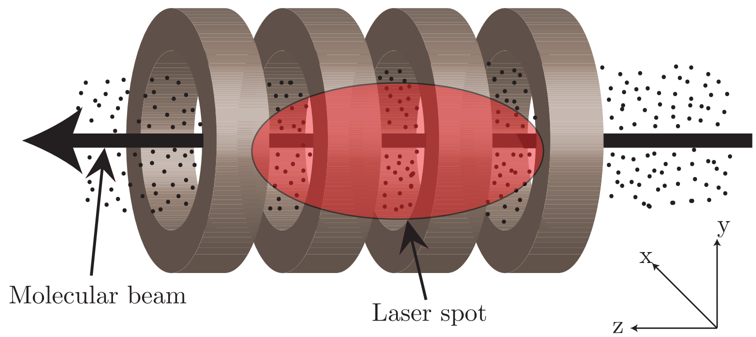

(a) Experiment/simulation geometry. Due to the blocking of the electrodes in the decelerator, the molecules do not experience a continuous light field.

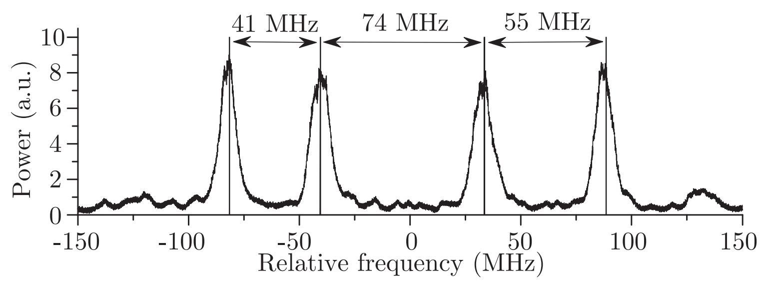

(b) The power broadened laser frequencies adressing the 4 hyperfine ground state levels, indicated by the vertical lines. Figure is adapted from [15]

Figure 4.5: Schematic of the experiment and the pump laser frequency characteristics.

4.2 Results

4.2.1 No electric field

Figure 4.6 shows the result of the first simulation program `srf_model.m`, which calls iteratively the corresponding function `srf.m` (see the appendices for the full codes of both programs). The two plots corresponds to the case (i) where both the $(J, F) = (1/2, 1)$ and $(1/2, 0)$ levels or case (ii) only the $(J, F) = (1/2, 1)$ level is/are excited. We call case (i) one sideband excitation and case (ii) two sideband excitation. Since there are no position dependent parameters in the model without an electric field, a single simulation of a molecule traveling through the light-field is sufficient. The figure shows a simulation for 30 by 30 s and L points, with maximum intensity $I_{max} = 0.5 I_s$ mW/cm^2 and interaction length $L_{max} = 0.03$ m. For every s and L, the program solves the rate equations for an arbitrary molecule starting at $z = -L/2$ and ending at $z = L/2$. The laser intensity is constant during the simulation. Practically, the electric field is abrubtly switched off when the molecular beam crosses the pump laser, by changing the voltage applied on the electrodes to zero. When the molecules have crossed the pump beam, the electric field can be switched on again by applying the voltage on the electrodes again. Molecules are not lost for trapping during this short switch-off.

The maximum gain which can be achieved for one sideband excitation is 26.4%. A large area can be distinguished surrounded by a 25% gain contour in figure 4.6a. The optimal saturation parameter s_{opt} where the highest gain can be reached is 0.03, which correspond to an optimal intensity $I_{opt} = 0.03 I_s = 0.09$ mW/cm^2. The optimal interaction length L_{opt} is 1.5 cm, although the maximum gain is not very sensitive to the interaction length near the maximum. If L is larger than this value, the same gain can be achieved with slightly lower intensity. Since the simulation is ran for a relative small range of L, and 30 s points are simulated, this cannot be seen in figure 4.6. The maximum gain for two sideband excitation is 28.6%. In this case $L_{opt} = 1.5$ cm and $s_{opt} = 0.03$.

High intensity

When the intensity gets too high, the gain in low-field seeking molecules decreases or even get negative. The laser sidebands become power broadened when the intensity is increased. The laser sideband addressing the $(J, F) = (1/2, 0)$ hyperfine level now can excite molecules from the $(J, F) = (3/2, 1)$

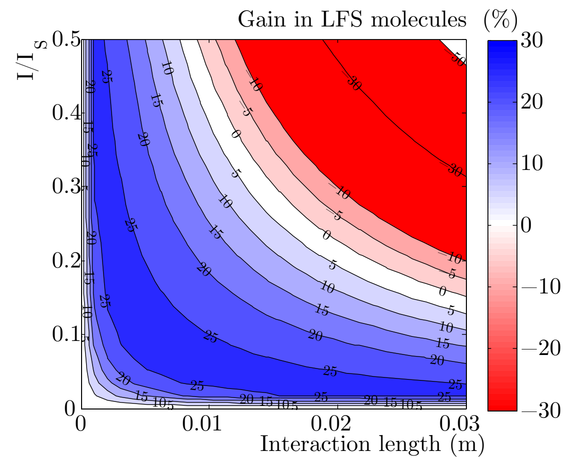

(a) One sideband excitation is applied which addresses the $J, F = (1/2, 1)$ manifold.

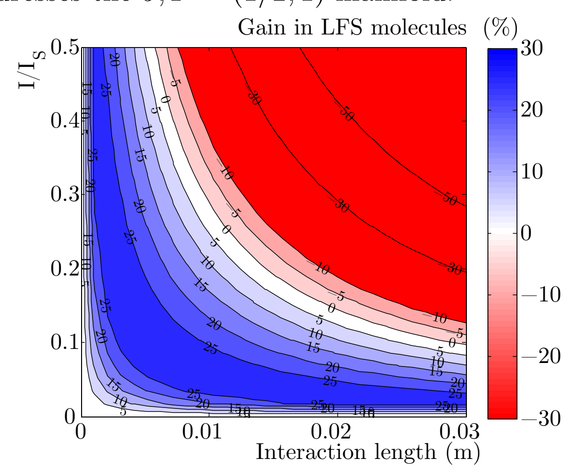

(b) Two sideband excitation is applied which address the $J, F = (1/2, 1)$ and $(1/2, 0)$ manifolds.

Figure 4.6: Gain in low-field seeking molecules without an electric field.

and ultimately from the $(J, F) = (3/2, 2)$ hyperfine levels. This effect is more clear when using two sidebands, since the frequency of the sideband addressing the $(1/2, 0)$ is closer to the low-field seeking hyperfine manifolds compared with the $(1/2, 1)$ sideband. Therefore, the gain becomes negative at lower L and s with two sideband excitation. Nevertheless, the maximum gain which can be achieved is higher when using two sideband excitation.

The effect of off-resonance excitation or cross excitation can be clearly seen in figure 4.7. In the set of plots at the top, the off-resonance excitation is neglected in the simulations. Despite the value for L, all curves asymptotical go to a gain of 44.5% for two sideband and 27.2% for one sideband excitation.

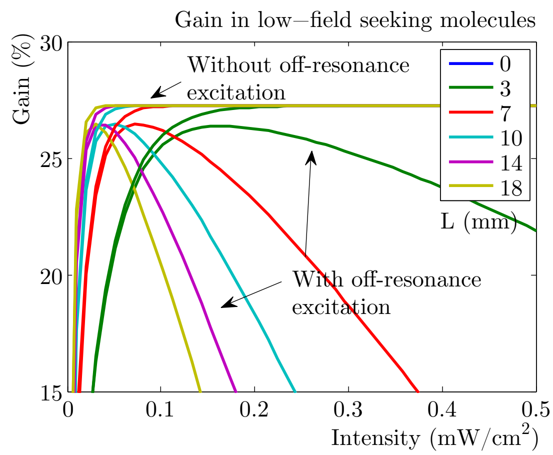

(a) One sideband excitation with and without off-resonance excitation.

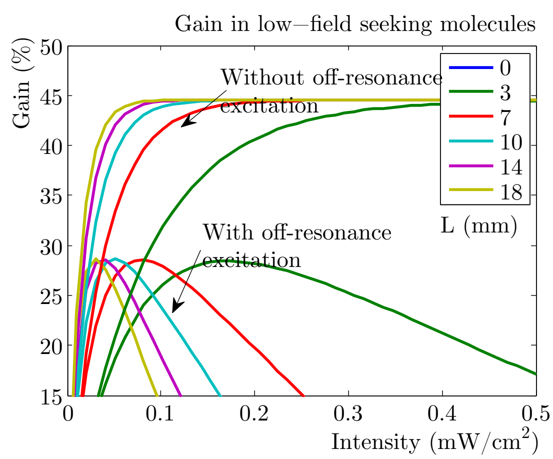

(b) Two sideband excitation with and without off-resonance excitation.

Figure 4.7: Gain in low-field seeking molecules without an electric field.

Branching ratio's

The above results which neglect off-resonance excitation is close what one would expect when we are dealing with a closed system, i.e. zero vibrational decay and constant branching. When neglecting off-resonance excitation and electronic branching ratio's, and set vibrational decay to zero, the maximum concentration in low-field seeking molecules for two sideband excitation would be 50.0%, since 4 out of 8 hyperfine magnetic sublevels within the $(J, F) = (3/2, 1)$ and $(3/2, 2)$ manifolds are low-field seeking. This would correspond to a gain of (see equation 4.5):

$$\text{Gain} = \frac{0.50 - 0.33}{0.33} \times 100\% = 50\% \tag{4.6}$$

The maximum gain without off-resonance excitation (see figure 4.7) is 44.5% for two sideband excitation according to the simulations. This means that the electronic and vibrational branching ratio's from table 3.1 and table 3.3 lead to a decrease of $50.0 - 44.5 = 5.5\%$ decrease in gain. For one sideband excitation this decrease is equal to $33.3 - 27.2 = 6.1\%$.

Interaction length

During the simulations, the only variable is the longitudinal z-coordinate of the molecules. The interaction length L determines the range of the z-coordinate for which the rate equations are solved. The maximum gain for both sideband configurations is at high L and low s. For even higher L and lower s, which fall outside the range of the simulation in figure 4.6, the maximum gain will slightly increase but remains ∼28.6% and ∼26.4% for both sidebands configurations. Without off-resonance excitation, the gain saturates to a maximum value at high intensity despite the interaction length. For a higher L this gain saturation is reached at lower intensity (see again figure 4.7). Obviously, if L is low, a higher intensity is needed in order to reach the maximum gain point. But on the other hand, a high intensity lead to off-resonance excitation, which suppresses the gain that will be reached. Finally, at zero interaction length the population in the low-field seeking states will not change: the gain is zero (blue line).

Laser power

Practically, the main limitation for hyperfine pumping is the limited available laser power. Currently, the same laser is used for hyperfine pumping at the beginning and detection at the end of the decelerator (the total power is split into two optical fibers). Moreover, a substantial amount of laser power is lost due to EOM and fiber incoupling. Before the pump laser is enterring the region where the molecues are, it passes two cylindrical lenses, an aperture and the electrodes of inside the vacuum chamber. Due to all of these losses, a maximum laser power of ∼1 mW can be used currently for the hyperfine pumping. The laser power P_{pump} at a given intensity I and interaction length L_{int}, is simply calculated as:

$$P_{pump} = I \times L_{int} \times L_{trans} \tag{4.7}$$

where L_{trans} is the height of the laser spot, which is taken to be ∼1.0 cm.

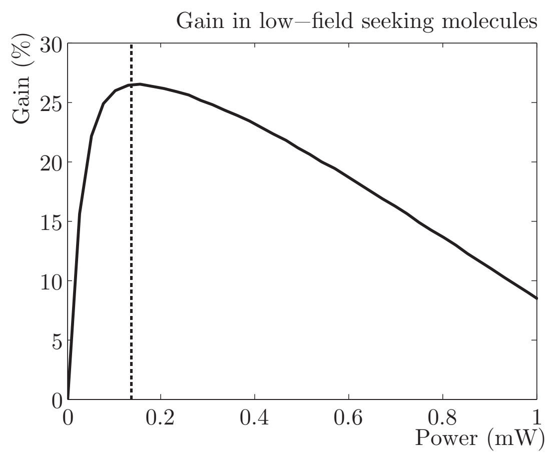

Figure 4.8: Gain in low-field seeking molecules as function of laser power, for two sideband excitation. Since the interaction length and laser intensity are inversely proportional, the gain can be plotted as function of laser power. Maximum gain is reached at $P_{pump} = 0.16$ mW.

For a constant laser power, doubling the s (or L) requires a decrease by half of the L (or s). Since L and s are related in this way, optimal $P_{pump,max}$ could be find to reach maximum gain (see figure 4.8), for an arbitrary choice of s. The optimal $P_{pump,max} = 0.16$ mW for one and two sideband excitation, which can be easily accomplished with the experimental resources which are available.

Magnetic field

A small magnetic field B applied during the hyperfine pumping can be of crucial importance for reaching significant gain in low-field seeking molecules.

When there would be no magnetic field, most of the molecules end up in the $(J, F) = (3/2, 2)$ manifold and the higher vibrational states. If the intensity of the laser is becoming higher, molecules in the $(J, F) = (3/2, 1)$ and $(3/2, 2)$ can be excited at some point. In this way molecules accumulate in the $M_F = 2$ and -2 sublevels of the $(J, F) = (3/2, 2)$ manifold. A magnetic field cause Larmor precession of the magnetic sublevels, which lead to remixing between the sublevels within a F-manifold.

It is difficult to calculate if it is beneficial to use a small magnetic field without a simulation. The remixing rate within each hyperfine manifold is different per manifold (see section 3.3.1). Moreover, the magnetic field induce a nonzero Zeeman shift of the magnetic sublevels with $M_F \neq 0$ (see equation 3.17). Figure 4.9 shows the dependence of the maximal gain as function of B for one and two sideband excitation. For each value of B, the maximum gain which can be achieved for 10 s and L points within the range of $s = 0 - 0.5$ and $L = 0 - 3.0$ cm is computed.

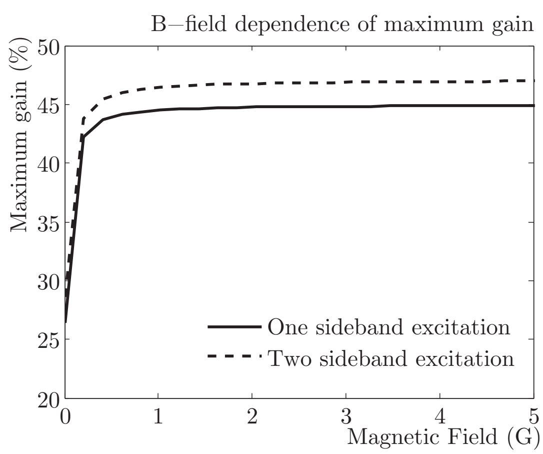

Figure 4.9: Maximum gain as function of magnetic field. The optimal magnetic field for both sideband configurations is ∼5 G.

Optimal $B = \sim 5$ G, which corresponds to the optimal magnetic field used for Doppler cooling [11]. When the magnetic field exeeds 6 G, the Doppler forces in [11] are reduced, because the magnetic field broadens the transitions, resulting in lower scattering rates. The broadening phenomena are not included in the simulations, since OBEs are obligatory to include power and magnetic field broadening. The gain which can be achieved with a 5 G magnetic field is 44.9% (one sideband excitation) and 47.0% (two sideband excitation). The s and L dependence of the gain with the magnetic field, is shown in figure 4.10. $s_{opt} = 0.13$ and $L_{opt} = 2.8$ cm, corresponding with a laser power of 1.1 mW.

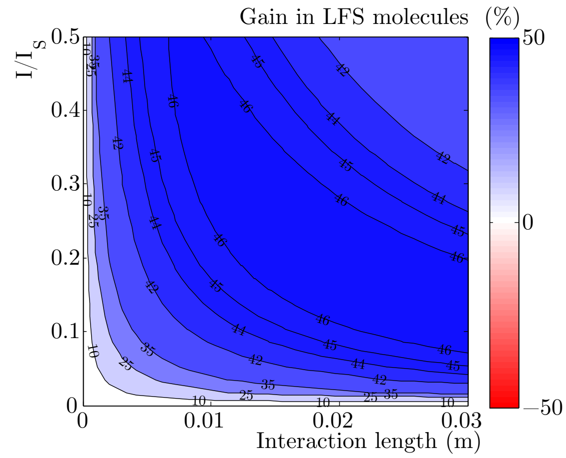

Figure 4.10: Gain in low-field seeking molecules for two sideband excitation and $B = 5$ G.

4.2.2 Electric field

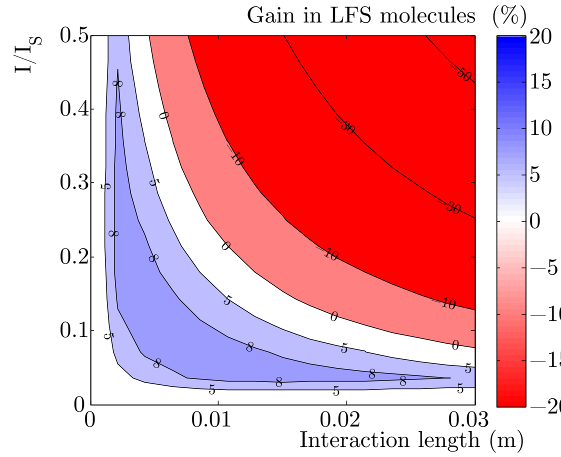

(a) One sideband excitation is applied which addresses the $J, F = (1/2, 1)$ manifold.

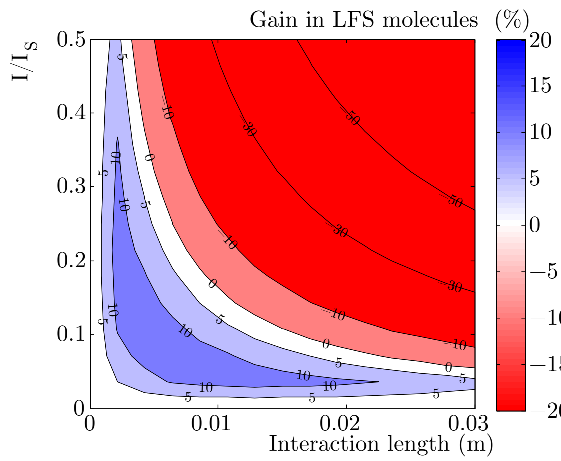

(b) Two sideband excitation is applied which address the $J, F = (1/2, 1)$ and $(1/2, 0)$ manifolds.

Figure 4.11: Gain in low-field seeking molecules with the application of an electric field. The voltage amplitude applied on the electrodes is 1 kV with distribution 1.

Figure 4.11 show the result of the simulation `srf_model_e_field`. The voltage amplitude is 1 kV. For two sideband excitation, which gave the highest gain for zero electric field (figure 4.6b), the maximum gain with an electric field is 12.3%. This is 16.3% less than the no electric field case. $s_{opt} = 0.04$, which correspond to $I_{opt} = 0.04 I_s = 0.12$ mW/cm^2, and $L_{opt} = 1.3$ cm. For one sideband excitation the maximum gain with an electric field is 9.3%, which is 17.1% lower compared without an electric field (figure 4.6b). For one sideband excitation, $s_{opt} = 0.04$ and $L_{opt} = 1.5$ cm.

Clearly, the gain is lower when the electric field is switched on. This can be explained by the Stark Shift which the molecules experience. The level-dependent Stark shift (figure 4.1) increases the detuning from resonance. When the detuning of the two bottom hyperfine levels is getting larger, the stimulated absorption/emission rates becomes smaller (section 3.2.2).

Magnetic field

When a 5 G magnetic field is applied during the hyperfine pumping, the gain in low-field seeking molecules can be even higher. Figure 4.12 show the result of the simulation with a 1 kV voltage amplitude electric field and $B = 5$ G for two sideband excitation. The maximum gain which can be achieved is 27.8% when $s_{opt} = 0.2$ and $L_{opt} = 3.0$ cm.

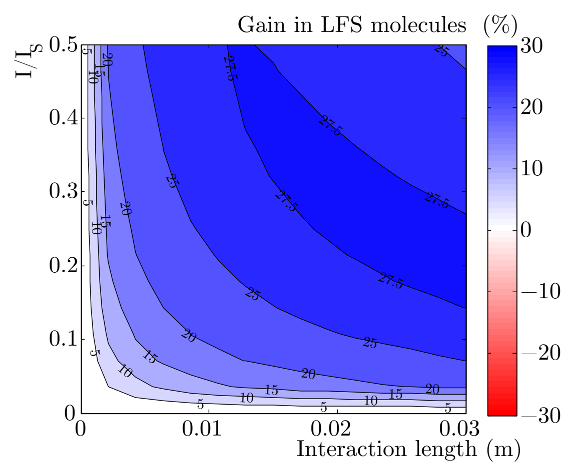

Figure 4.12: Gain in low-field seeking molecules with one sideband excitation, when the voltage amplitude is 1 kV and the magnetic field is 5 G.

The Zeeman splitting due to the magnetic field is order of magnitude lower than the characteristic Stark shift. The Zeeman splitting ΔE_{zeeman} (MHz) when $B = 5$ G, mean Stark shift ΔE_{stark} (MHz), hyperfine splitting Δhfs

and mean detuning δ_{mean} (MHz) for $B = 5$ G of all ground state hyperfine magnetic sublevels are shown in table 4.1. It can be clearly seen, that the

,

J	F	M_F	ΔE_{zeeman} (MHz)	ΔE_{stark} (MHz)	Δhfs	δ
		-2	7.0	56.0	170	233
		-1	3.5	3.7	170	177
3/2	2	0	0	3.7	170	174
		1	-3.5	3.7	170	170
		2	-7.0	56.0	170	219
		-1	5.8	56.0	129	191
3/2	1	0	0	3.7	129	133
		1	-5.8	56.0	129	179
1/2	0	0	0	56.0	55	111
		-1	-2.3	56.0	0	54
1/2	1	0	0	56.0	0	56
		1	2.3	56.0	0	58

Table 4.1: Zeeman splitting ΔE_{zeeman} (MHz), mean Stark shift ΔE_{stark} (MHz), hyperfine splitting Δhfs and mean detuning δ_{mean} (MHz) (radial units) of the ground state hyperfine magnetic sublevels when the voltage amplitude is 1 kV and $B = 5$ G. Only the $(J, F) = (1/2, 1)$ laser sideband is used (one sideband excitation). The blue (red) levels denote the low (high)-field seeking states.

Zeeman Shift does not have substantial influence on the detuning of the magnetic sublevels with one sideband excitation. The increased detuning of each level with the laser frequency, requires a higher s_{opt}, since the excitation rate of the levels decreases with increasing detuning. The gain with a magnetic field is higher due to the remixing effect of the magnetic field, following the same line of reasoning as in the no electric field case (see subsection 4.2.1). Nevertheless, it is better to switch off the electric field during the hyperfine pumping, since the maximum gain which can be increased is higher (see figure 4.9).

Voltage amplitude

For higher voltage amplitude applied on the electrodes of the traveling-wave decelerator, the gain decreases for all choices of s and L. The detuning between the laser frequency and the pump transitions become large due to the Stark shift of the molecules. The mean Stark shift of the molecules as function of the electric field strength is shown in table 4.2. The detuning

ΔE_{stark} (MHz)	low-field	high-field
$V = 1$ kV	3.7	55.8
$V = 1.5$ kV	-31	137
$V = 2.5$ kV	-190	430
$V = 5$ kV	-857	1492

Table 4.2: Mean Stark shifts ΔE_{stark} for some voltage amplitudes applied on the electrodes. The columns show the differential Stark shift for the low-field and high-field seeking Stark shifts in MHz (radial units).

of the hyperfine levels with the laser frequency is higher for higher voltage amplitudes, leading to lower excitation rates. Figure 4.13a and 4.13b show the result of the one sideband excitation simulation for 1.5 and 2.5 kV voltage amplitude, when $B = 5$ G. The results of the simulation for 1.5 kV are: maximum gain of 2.7% at $s_{opt} = 0.04$ and $L_{opt} = 0.8$ cm when $B = 5$ G. For a voltage amplitude of 2.5 kV the gain is negative for all choices of s and L. The electric field and corresponding Stark shift and detuning becomes too high at this voltage amplitude too pump molecules to the low-field seeking states. The results for electric field with voltage amplitude 5 kV are not shown since the gain is negative despite the choice of s and L.

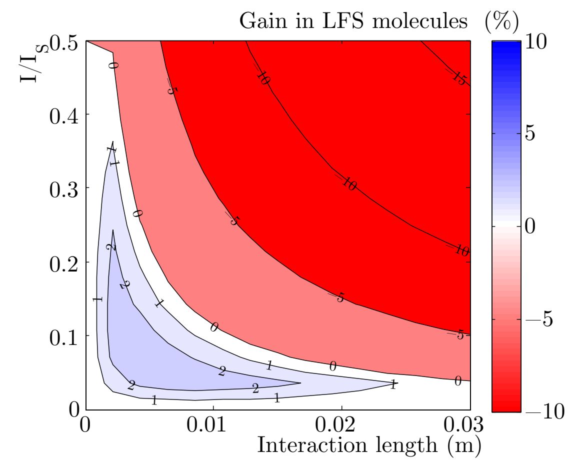

(a) Voltage amplitude is 1.5 kV.

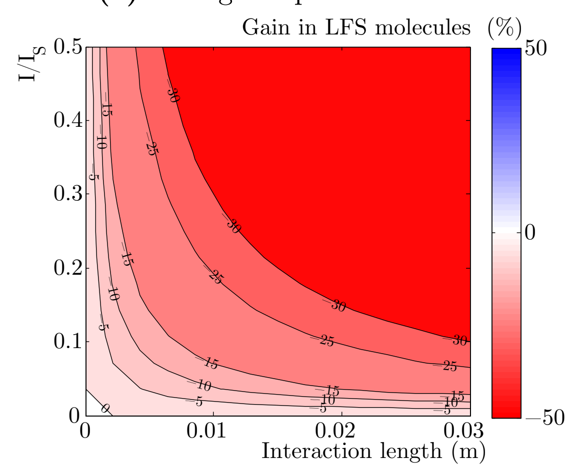

(b) Voltage amplitude is 2.5 kV.

Figure 4.13: Gain in low-field seeking molecules with one sideband excitation, when $B = 5$ G.

4.3 Conclusions

The best way to reach a optimum gain in low-field seeking molecules, is to switch off the electric field while the molecules propagate through the pump laser beam. The maximum gain which can be achieved is 47.0%, when $s = 0.13$ W/m^2, $L = \sim$2.8 cm and $B = 5$ G, using a laser with sidebands addressing the $(J, F) = (1/2, 1)$ and $(1/2, 0)$ hyperfine manifolds. The optimal laser power is 1.1 mW. The gain dynamics while varying the number of laser sidebands, laser intensity, interaction length and electric and magnetic field strength are simulated. The population dynamics and mechanisms behind these parameter are explored and discussed.

4.4 Discussion and possible improvements of the simulation

Obviously, the simulation described in the previous section gives a simplified picture of reality. The first thing to note is that the population dynamics are approached with rate equations instead of optical bloch equations, coherences are neglected. Since the steady state populations are the same in both approaches, small interaction lengths does not always give the steady state solutions and can therefore be different for the rate equation model compared to reality. Since in literature about atomic and molecular laser cooling or optical pumping rate equation models are used widely[17] [16] [14], it is expected that the rate equation model give reasonable solutions.

In the simulations it is assumed that there is a uniform transverse distribution of the molecules within the decelerator, regardless of the energytic state. Since the molecules only travelled 10 cm before entering the light field, it is expected that the distribution error is of secondary importance. After ablation the molecules have a nonzero transverse velocity spread according to a gaussian-shaped velocity distribution. Without deflection due to the electric field, the molecules would have a non-uniform transverse distribution after 10 cm deceleration. For a nonzero electric field, this effect becomes more important since the Stark shift in the decelerator is position dependent.

High-field seeking molecules near the electrodes which are pumped to a low-field seeking state, are still probable to crash to the walls despite the low-field seeking state they are in. The attracting force of the trap center could not be sufficient to deflect the molecule trajectory enough to prevent from crashing.

The electric field profiles inside the decelerator are not perfectly shaped traps. In the center of the trap, where the electric field is expected to be zero for all voltage amplitudes, there is a small bump, which can be seen in the plot for the high-field seeking ground state figure 4.4. It is unknown where this bump comes from.

The last important remark is the blocking of laser light due to the electrodes. Since the electrodes are 6 mm thick and are standing 9 mm apart, the computed interaction lengths have to be corrected with a factor $\frac{6}{6+9} = 0.4$. When the molecules are inside a ring-shaped electrode, the state of a individual molecule does not change since the decay probability of the $X^2\Sigma^+(v = 0, N = 1)$is very small. The population distribution of the state with 'electrode blocking' as function of z is shown in figure 4.14.

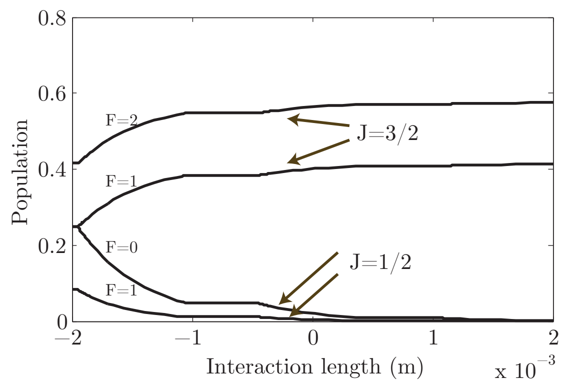

Figure 4.14: Population dynamics for a molecule passing the light field.

Chapter 5

Acknowledgements

Bibliography

[1] C.S. Wu et al. *Experimental test of parity conservation in beta decay*, PRL **105**, 1413 (1957)

[2] J.F. Barry et al. *Magneto-optical trapping of a diatomic molecule*, arXiv:1404.5680v1

[3] J.E. Van den Berg et al. *Travelling-wave deceleration of SrF Molecules*, submitted (2013)

[4] J.E. Van den Berg et al. *Deceleration and trapping of heavy diatomic molecules using a ring-decelerator*, Eur. Phys. J. D **66**: 235 (2012)

[5] J.E. Van den Berg *PhD thesis Concept chapter 1*, KVI internal document (2014)

[6] J.E. Van den Berg *Spectroscopic data of SrF and the use of* `PGOPHER`, KVI Groningen internal document (2011)

[7] J.F. Barry et al. *Laser Radiation Pressure Slowing of a Molecular Beam*, PRL **108**, 103002 (2012)

[8] J.F. Barry et al. *Laser cooling and slowing of a diatomic molecule*, PhD thesis (2013)

[9] R. Hoeppner et al. *A semiclassical optics derivation of Einstein's rate equations*, arXiv:1105.4120v1

[10] G. Grynberg et al. *An Introduction to Quantum Optics* p.99 (2010)

[11] E.S. Shuman et al. *Laser cooling of a diatomic molecule*, Nature **09443** (2010)

[12] D.J. Berkeland et al. *Destabilization of dark states and optical spectroscopy in Zeeman-degenerate atomic systems*, Phys. Rev. A, Vol. **65**, 033413 (2002)

[13] A.P.P. Van der Poel *Investigating cooling an deceleration of SrF molecules*, Master's Thesis (2012)

[14] T.E. Wall et al. *Lifetime of the A(v'=0) state and Franck-Condon factor of the A-X(0-0) transition of CaF measured by the saturation of laser-induced fluorescence*, Phys. Rev. A, Vol. **78**, 062509 (2008)

[15] C.E. Rogers III *Creation of arbitrary spectra with an electro-optic modulator*, arXiv:1011.5169v1

[16] M.R. Tarbutt et al. *Design for a fountain of YbF molecules to measure the electrons electric dipole moment*, New. Journ. Of Phys. **15**, 053034 (2013)

[17] *Radiative force from optical cycling on a diatomic molecule*, PRL **103**, 223001 (2009)

[18] H.J. Metcalf, P. Van der Straten *Laser cooling and trapping*, Springer (1999)

[19] B.K. Stuhl et al. *Magneto-optical trap for polar molecules*, PRL **101**, 243002 (2008)

Appendix A

Laser system

A.1 Setting up new detection system

For the hyperfine state pumping at the beginning of the decelerator, a new detection- and optical pumping system is made between ablation and the first half meter of the decelerator. Since the performance of the decelerator is very sensitive to changes within the setup (gas valve position, decelerator allignment, pill quality etc.), a intermediate detection system enables the possibility to detect molecules before they reach the end of the decelerator. When molecules can be detected before they enter or have just enterred the decelerator, potential problems with, within or before the source chamber could be excluded. Moreover, for the optical pumping described in chapter 4 a laser through the ring-shaped electrodes has to be set up. The same $X^2\Sigma^+(v = 0, N = 1) \rightarrow A^2\Pi_{1/2}(v' = 0, J' = 1/2^+)$ transition is used for both detection and pumping.

A.1.1 Collimating the laser beam

The main challenge for detection molecule at the begin of the decelerator, is collimating the laser beam in such a way that the laser beam goes exactly through two electrodes. Resulting stray light coming from reflections with the electrodes or the rods make detection impossible. Therefore, a laser beam with a width smaller than the 0.9 mm spacing between consecutive electrodes and a height smaller than the 10 mm spacing between two perpendicular rods with respect to the laser beam should be sufficient. A circular laser spot with radius $<$ 0.9 mm will result in a relative small interaction area, wheras molecules are spread out over the whole cross-section of the electrodes. Therefore, cylindrical lenses can be used to converge or divergerce incoming parallel light in one direction. Since the optical system has to be installed outside the vacuum chamber i.e. at least 25 cm away from the electrodes, diffraction phenomena eliminate the use of slits or appertures.

663 nm laser light with sidebands matching the hyperfine levels of the $X^2\Sigma^+(v = 0, N = 1)$state, is transported to the decelerator by an optical fiber. The radius of the laser spot is ∼4 mm. Two mirrors are used to adjust the transverse and longitudinal position of the beam before entering the vacuum chamber. Two cyclindrical lenses of focal length (f) −3.9 mm and 25.4 mm make the beam broader in the longitudinal direction. A conventional spherical lens of $f = 30.0$ cm converges the beam in both directions, in order to make an rectangular image of width ∼0.9 mm and height of ∼4.0 mm at the electrode position in the vacuum chamber. The outcoming diverging beam after passing the electrodes can be identified at the other side of the vacuum chamber. In this way the laser beam can be aligned perpendicular to the molecular beam axis. The two consecutive electrodes through which the laser beam propagates can be adjusted by changing the orientation of both mirrors.

Spontaneous emission of SrF molecules enables the possibility to detect SrF molecules. In our research we use either the $v' = 0 \rightarrow v" = 0$ (663 nm) transition for excitation/detection or $v' = 0 \rightarrow v" = 1$ (685 nm) transition for detection. This enables two different detection schemes. For example, when the 663 nm laser is used for hyperfine pumping at the beginning of the decelerator, spontaneous 685 nm decay can be measured simultaneously. When the laser is shining through the rings of the decelerator, stray light of 663 nm makes resonant detection impossible. Figure **??** shows a detection signal using the new detection system.

Appendix B

'srf.m'

```
function [dN] = SRF(z,N,I,delta,B,fc,gamma,Gamma,rmr,v,s)
% N(i) are the populations in the ground state sublevels i=1:12,
% excited state sublevels i=13:16 and higher vibrational states i=17

% R(i,j) is the stimulated absorption/emission rate of laser frequency i
% with ground state sublevel j

dN=zeros(17,1); A=ones(4,12); R=zeros(4,12);

% select the sidebands to be pumped
if s(1,1)==0; A(1,:)=0; end
if s(1,2)==0; A(2,:)=0; end
if s(1,3)==0; A(3,:)=0; end
if s(1,4)==0; A(4,:)=0; end

% UNCOMMENT: no off-resonance excitation
% A(1,4:12)=0; A(2,1:3)=0; A(2,5:12)=0; A(3,1:4)=0; A(3,8:12); A(4,1:7);
% UNCOMMENT: prevent dark states to be pumped
A(:,8)=0; A(:,12)=0;
%% stimulated absorption and emission rates
R(1,1)=fc*B(2,1)*A(1,1)*((gamma)*I)/((1+((4*delta(1,1)^2)/((Gamma)^2))));
R(1,2)=fc*B(1,2)*A(1,2)*((gamma)*I)/((1+((4*delta(1,2)^2)/((Gamma)^2))));
R(1,3)=fc*B(4,3)*A(1,3)*((gamma)*I)/((1+((4*delta(1,3)^2)/((Gamma)^2))));
R(1,4)=fc*B(3,4)*A(1,4)*((gamma)*I)/((1+((4*delta(1,4)^2)/((Gamma)^2))));
R(1,5)=fc*B(2,5)*A(1,5)*((gamma)*I)/((1+((4*delta(1,5)^2)/((Gamma)^2))));
R(1,6)=fc*B(1,6)*A(1,6)*((gamma)*I)/((1+((4*delta(1,6)^2)/((Gamma)^2))));
R(1,7)=fc*B(4,7)*A(1,7)*((gamma)*I)/((1+((4*delta(1,7)^2)/((Gamma)^2))));
R(1,8)=fc*B(1,8)*A(1,8)*((gamma)*I)/((1+((4*delta(1,8)^2)/((Gamma)^2))));
R(1,9)=fc*B(2,9)*A(1,9)*((gamma)*I)/((1+((4*delta(1,9)^2)/((Gamma)^2))));
R(1,10)=fc*B(3,10)*A(1,10)*((gamma)*I)/((1+((4*delta(1,10)^2)/((Gamma)^2))));
R(1,11)=fc*B(4,11)*A(1,11)*((gamma)*I)/((1+((4*delta(1,11)^2)/((Gamma)^2))));
R(1,12)=fc*B(1,12)*A(1,12)*((gamma)*I)/((1+((4*delta(1,12)^2)/((Gamma)^2))));

R(2,1)=fc*B(2,1)*A(2,1)*((gamma)*I)/((1+((4*delta(2,1)^2)/((Gamma)^2))));
R(2,2)=fc*B(1,2)*A(2,2)*((gamma)*I)/((1+((4*delta(2,2)^2)/((Gamma)^2))));
R(2,3)=fc*B(4,3)*A(2,3)*((gamma)*I)/((1+((4*delta(2,3)^2)/((Gamma)^2))));
R(2,4)=fc*B(3,4)*A(2,4)*((gamma)*I)/((1+((4*delta(2,4)^2)/((Gamma)^2))));
R(2,5)=fc*B(2,5)*A(2,5)*((gamma)*I)/((1+((4*delta(2,5)^2)/((Gamma)^2))));
R(2,6)=fc*B(1,6)*A(2,6)*((gamma)*I)/((1+((4*delta(2,6)^2)/((Gamma)^2))));
R(2,7)=fc*B(4,7)*A(2,7)*((gamma)*I)/((1+((4*delta(2,7)^2)/((Gamma)^2))));
R(2,8)=fc*B(1,8)*A(2,8)*((gamma)*I)/((1+((4*delta(2,8)^2)/((Gamma)^2))));
R(2,9)=fc*B(2,9)*A(2,9)*((gamma)*I)/((1+((4*delta(2,9)^2)/((Gamma)^2))));
R(2,10)=fc*B(3,10)*A(2,10)*((gamma)*I)/((1+((4*delta(2,10)^2)/((Gamma)^2))));
R(2,11)=fc*B(4,11)*A(2,11)*((gamma)*I)/((1+((4*delta(2,11)^2)/((Gamma)^2))));
R(2,12)=fc*B(1,12)*A(2,12)*((gamma)*I)/((1+((4*delta(2,12)^2)/((Gamma)^2))));

R(3,1)=fc*B(2,1)*A(3,1)*((gamma)*I)/((1+((4*delta(3,1)^2)/((Gamma)^2))));
R(3,2)=fc*B(1,2)*A(3,2)*((gamma)*I)/((1+((4*delta(3,2)^2)/((Gamma)^2))));
R(3,3)=fc*B(4,3)*A(3,3)*((gamma)*I)/((1+((4*delta(3,3)^2)/((Gamma)^2))));
R(3,4)=fc*B(3,4)*A(3,4)*((gamma)*I)/((1+((4*delta(3,4)^2)/((Gamma)^2))));
R(3,5)=fc*B(2,5)*A(3,5)*((gamma)*I)/((1+((4*delta(3,5)^2)/((Gamma)^2))));
```

```
R(3,6)=fc*B(1,6)*A(3,6)*((gamma)*I)/((1+((4*delta(3,6)^2)/((Gamma)^2))));
R(3,7)=fc*B(4,7)*A(3,7)*((gamma)*I)/((1+((4*delta(3,7)^2)/((Gamma)^2))));
R(3,8)=fc*B(1,8)*A(3,8)*((gamma)*I)/((1+((4*delta(3,8)^2)/((Gamma)^2))));
R(3,9)=fc*B(2,9)*A(3,9)*((gamma)*I)/((1+((4*delta(3,9)^2)/((Gamma)^2))));
R(3,10)=fc*B(3,10)*A(3,10)*((gamma)*I)/((1+((4*delta(3,10)^2)/((Gamma)^2))));
R(3,11)=fc*B(4,11)*A(3,11)*((gamma)*I)/((1+((4*delta(3,11)^2)/((Gamma)^2))));
R(3,12)=fc*B(1,12)*A(3,12)*((gamma)*I)/((1+((4*delta(3,12)^2)/((Gamma)^2))));

R(4,1)=fc*B(2,1)*A(4,1)*((gamma)*I)/((1+((4*delta(4,1)^2)/((Gamma)^2))));
R(4,2)=fc*B(1,2)*A(4,2)*((gamma)*I)/((1+((4*delta(4,2)^2)/((Gamma)^2))));
R(4,3)=fc*B(4,3)*A(4,3)*((gamma)*I)/((1+((4*delta(4,3)^2)/((Gamma)^2))));
R(4,4)=fc*B(3,4)*A(4,4)*((gamma)*I)/((1+((4*delta(4,4)^2)/((Gamma)^2))));
R(4,5)=fc*B(2,5)*A(4,5)*((gamma)*I)/((1+((4*delta(4,5)^2)/((Gamma)^2))));
R(4,6)=fc*B(1,6)*A(4,6)*((gamma)*I)/((1+((4*delta(4,6)^2)/((Gamma)^2))));
R(4,7)=fc*B(4,7)*A(4,7)*((gamma)*I)/((1+((4*delta(4,7)^2)/((Gamma)^2))));
R(4,8)=fc*B(1,8)*A(4,8)*((gamma)*I)/((1+((4*delta(4,8)^2)/((Gamma)^2))));
R(4,9)=fc*B(2,9)*A(4,9)*((gamma)*I)/((1+((4*delta(4,9)^2)/((Gamma)^2))));
R(4,10)=fc*B(3,10)*A(4,10)*((gamma)*I)/((1+((4*delta(4,10)^2)/((Gamma)^2))));
R(4,11)=fc*B(4,11)*A(4,11)*((gamma)*I)/((1+((4*delta(4,11)^2)/((Gamma)^2))));
R(4,12)=fc*B(1,12)*A(4,12)*((gamma)*I)/((1+((4*delta(4,12)^2)/((Gamma)^2))));
%% multi-level rate equations
dN(1)=  (1/v)*(sum(R(:,1)*(N(14)-N(1)))    +fc*(gamma)*(B(1,1)*N(13)+B(2,1)*N(14)+
    B(3,1)*N(15)+B(4,1)*N(16))        -rmr(1)*(N(1)-N(2)));
dN(2)=  (1/v)*(sum(R(:,2)*(N(13)-N(2)))    +fc*(gamma)*(B(1,2)*N(13)+B(2,2)*N(14)+
    B(3,2)*N(15)+B(4,2)*N(16))        -rmr(1)*(2*N(2)-N(1)-N(3)));
dN(3)=  (1/v)*(sum(R(:,3)*(N(16)-N(3)))    +fc*(gamma)*(B(1,3)*N(13)+B(2,3)*N(14)+
    B(3,3)*N(15)+B(4,3)*N(16))        -rmr(1)*(N(3)-N(2)));
dN(4)=  (1/v)*(sum(R(:,4)*(N(15)-N(4)))    +fc*(gamma)*(B(1,4)*N(13)+B(2,4)*N(14)+
    B(3,4)*N(15)+B(4,4)*N(16)));
dN(5)=  (1/v)*(sum(R(:,5)*(N(14)-N(5)))    +fc*(gamma)*(B(1,5)*N(13)+B(2,5)*N(14)+
    B(3,5)*N(15)+B(4,5)*N(16))        -rmr(3)*(N(5)-N(6)));
dN(6)=  (1/v)*(sum(R(:,6)*(N(13)-N(6)))    +fc*(gamma)*(B(1,6)*N(13)+B(2,6)*N(14)+
    B(3,6)*N(15)+B(4,6)*N(16))        -rmr(3)*(2*N(6)-N(5)-N(7)));
dN(7)=  (1/v)*(sum(R(:,7)*(N(16)-N(7)))    +fc*(gamma)*(B(1,7)*N(13)+B(2,7)*N(14)+
    B(3,7)*N(15)+B(4,7)*N(16))        -rmr(3)*(N(7)-N(6)));
dN(8)=  (1/v)*(sum(R(:,8)*(N(8)))          +fc*(gamma)*(B(1,8)*N(13)+B(2,8)*N(14)+
    B(3,8)*N(15)+B(4,8)*N(16))        -rmr(4)*(N(8)-N(9)));
dN(9)=  (1/v)*(sum(R(:,9)*(N(14)-N(9)))    +fc*(gamma)*(B(1,9)*N(13)+B(2,9)*N(14)+
    B(3,9)*N(15)+B(4,9)*N(16))        -rmr(4)*(2*N(9)-N(8)-N(10)));
dN(10)= (1/v)*(sum(R(:,10)*(N(15)-N(10))) +fc*(gamma)*(B(1,10)*N(13)+B(2,10)*N
    (14)+B(3,10)*N(15)+B(4,10)*N(16))  -rmr(4)*(2*N(10)-N(9)-N(11)));
dN(11)= (1/v)*(sum(R(:,11)*(N(16)-N(11))) +fc*(gamma)*(B(1,11)*N(13)+B(2,11)*N
    (14)+B(3,11)*N(15)+B(4,11)*N(16))  -rmr(4)*(2*N(11)-N(10)-N(12)));
dN(12)= (1/v)*(sum(R(:,12)*(N(12)))       +fc*(gamma)*(B(1,12)*N(13)+B(2,12)*N
    (14)+B(3,12)*N(15)+B(4,12)*N(16))  -rmr(4)*(N(12)-N(11)));

dN(13)= (1/v)*(-(sum(R(:,2)*(N(13)-N(2)))+sum(R(:,6)*(N(13)-N(6))))
                                        -(gamma)*N(13));
dN(14)= (1/v)*(-(sum(R(:,1)*(N(14)-N(1)))+sum(R(:,5)*(N(14)-N(5)))+sum(R(:,9)*(N
    (14)-N(9))))        -(gamma)*N(14));
dN(15)= (1/v)*(-(sum(R(:,4)*(N(15)-N(4)))+sum(R(:,10)*(N(15)-N(10))))
                                      -(gamma)*N(15));
dN(16)= (1/v)*(-(sum(R(:,3)*(N(16)-N(3)))+sum(R(:,7)*(N(16)-N(7)))+sum(R(:,11)*(N
    (16)-N(11))))      -(gamma)*N(16));

dN(17)= (1/v)*((1-fc)*(gamma)*(N(13)+N(14)+N(15)+N(16)));
end
```

Appendix C

'srf_model.m'

```
% this program solves the hyperfine pumping rate equations for SrF, using
% only one 663 nm pump laser. The input is max_L, max_intensity, N1, N2,
% Intenity and L. This program solves the function 'srf.m' for all input
% points. The output vectors are 'Intensity', 'L', and the matrix 'gain'.

clear all; close all;
%% parameters for simulation
N1=30; %number of intensity points
N2=30; %number of interaction length points
s(1,1)=1; %sideband (J,F)=(1/2,1) on (=1) or off (=0)
s(1,2)=1; %sideband (J,F)=(1/2,0) on (=1) or off (=0)
s(1,3)=0; %sideband (J,F)=(3/2,1) on (=1) or off (=0)
s(1,4)=0; %sideband (J,F)=(3/2,2) on (=1) or off (=0)
max_intensity=0.5; %maximal intensity point in I/I_s
max_L=3e-2; %maximal interaction length point
%% initial conditions
Intensity=linspace(0,max_intensity,N1); %generate the intensity points
L=linspace(0,max_L,N2); %generate interaction length point
gamma=1/(24.1e-9); %spontaneous emission rate in Hz
Gamma=gamma; %natural linewidth in rad/s
v=370; %initial velocity in m/s
h=6.626e-34; %planck's constant in SI-units
c=2.998e8; %speed of light in SI-units
labda=663.3e-9; %transition wavelength in m
fc=0.9814; %franck-condon factor
ub=9.27400968e-24; %bohr magneton in J/T
B=5e-4; %magnetic field in T
g=[-0.33 0 0.83 0.5]; %g-factors
rmr=abs(g.*ub.*B./h)     %remixing rate in Hz
zs=-(g.*ub.*B./h) %zeeman splittings in rad/s
I_s=(pi*h*c*gamma)/(3*(labda^3)); %saturation intensity in W/m^2

delta=zeros(4,12); %delta(i,j) is the detuning for laser frequency i with
                   %sublevel j. i=1 coincide with (J,F)=(1/2,1). j=1
                   %coincide with (J,F,MF)=(1/2,1,-1). Delta in rad/s.
delta(1,1)=0-zs(1); delta(1,2)=0; delta(1,3)=0+zs(1); delta(1,4)=55e6;
delta(1,5)=129e6-zs(3); delta(1,6)=129e6; delta(1,7)=129e6+zs(3); delta(1,8)=170
    e6-2*zs(4);
delta(1,9)=170e6-zs(4); delta(1,10)=170e6; delta(1,11)=170e6+zs(4); delta(1,12)
    =170e6+2*zs(4);
delta(2,1)=55e6-zs(1); delta(2,2)=55e6; delta(2,3)=55e6+zs(1); delta(2,4)=0;
delta(2,5)=74e6-zs(3); delta(2,6)=74e6; delta(2,7)=74e6+zs(3); delta(2,8)=115e6
    -2*zs(4);
delta(2,9)=115e6-zs(4); delta(2,10)=115e6; delta(2,11)=115e6+zs(4); delta(2,12)
    =115e6+2*zs(4);
delta(3,1)=129e6; delta(3,2)=delta(3,1); delta(3,3)=delta(3,1);
delta(3,4)=74e6; delta(3,5)=0; delta(3,7)=delta(3,5); delta(3,6)=0;
delta(3,8)=41e6; delta(3,12)=delta(3,8); delta(3,9)=41e6;
delta(3,10)=delta(3,9); delta(3,11)=delta(3,9); delta(4,1)=170e6;
delta(4,2)=delta(4,1); delta(4,3)=delta(4,1); delta(4,4)=115e6;
delta(4,5)=41e6; delta(4,7)=delta(2,5); delta(4,6)=41e6; delta(4,8)=0;
```

```
delta(4,12)=delta(4,8); delta(4,9)=0; delta(4,10)=delta(4,9);
delta(4,11)=delta(4,9)

B=zeros(4,12); %B(k,j) is the branching ratio for decay of excited state
               %sublevel k to ground state sublevel j. k=1 coincide with
               %(F,MF)=(0,0). j=1 coincide with (J,F,MF)=(1/2,1,-1).
B(1,1)=1/6; B(1,2)=1/6; B(1,3)=1/6; B(1,4)=0; B(1,5)=1/6; B(1,6)=1/6;
B(1,7)=1/6; B(1,8)=0; B(1,9)=0; B(1,10)=0; B(1,11)=0; B(1,12)=0;
B(2,1)=1/8; B(2,2)=1/8; B(2,3)=0; B(2,4)=1/12; B(2,5)=1/8; B(2,6)=1/8;
B(2,7)=0; B(2,8)=1/4; B(2,9)=1/8; B(2,10)=1/24; B(2,11)=0; B(2,12)=0;
B(3,1)=1/8; B(3,2)=0; B(3,3)=1/8; B(3,4)=1/12; B(3,5)=1/8; B(3,6)=0;
B(3,7)=1/8; B(3,8)=0; B(3,9)=1/8; B(3,10)=1/6; B(3,11)=1/8; B(3,12)=0;
B(4,1)=0; B(4,2)=1/8; B(4,3)=1/8; B(4,4)=1/12; B(4,5)=0; B(4,6)=1/8;
B(4,7)=1/8; B(4,8)=0; B(4,9)=0; B(4,10)=1/24; B(4,11)=1/8; B(4,12)=1/4;
%% simulation
for n1=1:1:N1
        for n2=1:1:N2
        formatSpec = 'Intensity is %f, L is %f m, n1 is %f, n2 is %f \n';
        fprintf(formatSpec,Intensity(n1),L(n2),n1,n2)
        if L(n2)>0
        initial(1:12)=1/12; initial(13:17)=0; %initial concentrations of
                                              %ground states 1:12, excited
                                              % states 13:16 and v">0 17
        ns=s(1,1)+s(1,2)+s(1,3)+s(1,4); %number of sidebands
        I=Intensity(n1)/ns; %define intensity per sideband
        range=[-L(n2)/2 L(n2)/2]; %define interaction zone
        [Z,P]=ode15s(@(z,N) SRF(z,N,I,delta,B,fc,gamma,Gamma,rmr,v,s),range,
            initial);
        % UNCOMMENT: see the population dynamics (solution of MLRE)
        %           make sure N1=N2=1 and define one Intensity and L point
        %           of interest
%           HFS=P(:,1)+P(:,2)+P(:,3)+P(:,4)+P(:,5)+P(:,7)+P(:,8)+P(:,12)
%           LFS=P(:,6)+P(:,9)+P(:,10)+P(:,11)
%           ES=P(:,13)+P(:,14)+P(:,15)+P(:,16)
%           HVS=P(:,17)
%           DS=P(:,8)+P(:,12)
%           plot(Z,F1,'b',Z,F2,'r',Z,F3,'g',Z,F4,'k'); legend; figure;
%           plot(Z,HFS,'r',Z,LFS,'b',Z,HVS,'c',Z,DS,'k',Z,ES,'y'); figure;
        gain(n1,n2)=(((P(end,6)+sum(P(end,(9:11))))-(1/3))/(1/3))*100;
        clear Z P
        else
        gain(n1,n2)=0;
        end
        end
end
%% plotting
set(gca,'FontSize',20);
contourf(L,Intensity,gain); xlabel('Interaction length (mm)');
ylabel('I/I_s'); title('Gain in LFS molecules (%)'); colorbar;
h=colorbar; set(h,'fontsize',20);
% UNCOMMENT: 2D plotting (optional)
% figure; set(gca,'FontSize',20);
% plot(Intensity,gain(:,1:N2)); xlabel('I/I_s');
%% data acquisition
% UNCOMMENT: save the parameter vectors and the gain matrix
name = ['data/gain_',num2str(N1),'_I_points_',num2str(N2),'_L_points_',num2str(
    sum(s)),'_sidebands_max_intensity_',num2str(max_intensity),'
    _max_interaction_length_',num2str(max_L),'_B_field_0.0005.mat']
save(name,'I_s','B','s','Intensity','L','gain')
```

Appendix D

'srf_model_e_field.m'

```
% this program solves the hyperfine pumping rate equations for SrF, using
% only one 663 nm pump laser. The input is max_L, max_intensity, N1, N2,
% Intenity and L. This program solves the function 'srf.m' for all input
% points. The output vectors are 'Intensity', 'L', and the matrix 'gain'.
%
% In this program the electric field in the decelerator is not switched
% off, i.e. the molecules experience a stark shift. The simulation is
% build up as follows:
%
% - The electric field and corresponding stark shift of one trap
% (potential well) is calculated using makeEfield.m, run_makeEfield.m,
% Calculate_stark_shift, calcStarkShift.m.
%
% - Stark_shift_one_trap_?_kV_distr_?.m (? is the voltage and distribution
% of the waveforms for the amplifiers) calculate the stark shift of 10x10
% linear grid points of this single trap.
%
% - For each parameter point the simulation is ran for all these 100 points
% with its corresponding stark shift and resulting detuning
clear all; close all;
%% parameters for simulation
N1=15; %number of intensity points
N2=15; %number of interaction length points
s(1,1)=1; %sideband (J,F)=(1/2,1) on (=1) or off (=0)
s(1,2)=0; %sideband (J,F)=(1/2,0) on (=1) or off (=0)
s(1,3)=0; %sideband (J,F)=(3/2,1) on (=1) or off (=0)
s(1,4)=0; %sideband (J,F)=(3/2,2) on (=1) or off (=0)
max_intensity=0.5; %maximal intensity point in I/I_s
max_L=3e-2; %maximal interaction length point
volt=2.5; %amplitude of the waveforms
distr=1; %1=AC guiding, 5=DC guiding
%% load relevant files
name=['..\Stark_Shift\stark_shift_',num2str(volt),'_kV_distr_',...
    num2str(distr),'_sp.mat'];
load(name) %load corresponding stark shift
%% initial conditions
Intensity=linspace(0,max_intensity,N1); %generate the intensity points
L=linspace(0,max_L,N2); %generate interaction length point
gamma=1/(24.1e-9); %spontaneous emission rate in Hz
Gamma=gamma; %natural linewidth in rad/s
v=370; %initial velocity in m/s
h=6.626e-34; %planck's constant in SI-units
c=2.998e8; %speed of light in SI-units
labda=663.3e-9; %transition wavelength in m
fc=0.9814; %franck-condon factor
ub=9.27400968e-24; %bohr magneton in J/T
B=5e-4; %magnetic field in T
g=[-0.33 0 0.83 0.5]; %g-factors
rmr=abs(g.*ub.*B./h); %remixing rate in Hz
zs=-(g.*ub.*B./h) %zeeman splittings in rad/s
I_s=(pi*h*c*gamma)/(3*(labda^3)); %saturation intensity in W/m^2
```

```
B=zeros(4,12); %B(k,j) is the branching ratio for decay of excited state
               %sublevel k to ground state sublevel j. k=1 coincide with
               %(F,MF)=(0,0). j=1 coincide with (J,F,MF)=(1/2,1,-1).
B(1,1)=1/6; B(1,2)=1/6; B(1,3)=1/6; B(1,4)=0; B(1,5)=1/6; B(1,6)=1/6;
B(1,7)=1/6; B(1,8)=0; B(1,9)=0; B(1,10)=0; B(1,11)=0; B(1,12)=0;
B(2,1)=1/8; B(2,2)=1/8; B(2,3)=0; B(2,4)=1/12; B(2,5)=1/8; B(2,6)=1/8;
B(2,7)=0; B(2,8)=1/4; B(2,9)=1/8; B(2,10)=1/24; B(2,11)=0; B(2,12)=0;
B(3,1)=1/8; B(3,2)=0; B(3,3)=1/8; B(3,4)=1/12; B(3,5)=1/8; B(3,6)=0;
B(3,7)=1/8; B(3,8)=0; B(3,9)=1/8; B(3,10)=1/6; B(3,11)=1/8; B(3,12)=0;
B(4,1)=0; B(4,2)=1/8; B(4,3)=1/8; B(4,4)=1/12; B(4,5)=0; B(4,6)=1/8;
B(4,7)=1/8; B(4,8)=0; B(4,9)=0; B(4,10)=1/24; B(4,11)=1/8; B(4,12)=1/4;
%% simulation
 for n1=1:1:N1
        for n2=1:1:N2
        formatSpec = 'Intensity is %f, L is %f m, n1 is %f, n2 is %f \n';
        fprintf(formatSpec,Intensity(n1),L(n2),n1,n2)
                for n0=1:1:size(lfs,2);
                delta=zeros(4,12); %delta(i,j) is the detuning for laser
                                   %frequency i with sublevel j. i=1
                                   %coincide with (J,F)=(1/2,1). j=1
                                   %coincide with (J,F,MF)=(1/2,1,-1).
                                   %lfs(n0)/hfs(n0) is the
                                   %lfs/hfs stark shift of molecule n0
                delta(1,1)=hfs(n0)-zs(1); delta(1,2)=hfs(n0);
                delta(1,3)=delta(1,1)+2*zs(1); delta(1,4)=55e6+hfs(n0);
                delta(1,5)=129e6+hfs(n0)-zs(3); delta(1,7)=delta(1,5)+2*zs(3);
                delta(1,6)=129e6+lfs(n0); delta(1,8)=170e6+hfs(n0)-2*zs(4);
                delta(1,12)=delta(1,8)+4*zs(4); delta(1,9)=170e6+lfs(n0)-zs(4);
                delta(1,10)=170e6+lfs(n0); delta(1,11)=delta(1,9)+2*zs(4);
                delta(2,1)=-55e6+hfs(n0)-zs(1); delta(2,2)=-55e6+hfs(n0);
                delta(2,3)=delta(2,1)+2*zs(1); delta(2,4)=hfs(n0);
                delta(2,5)=74e6+hfs(n0)-zs(3); delta(2,7)=delta(2,5)+2*zs(3);
                delta(2,6)=74e6+lfs(n0); delta(2,8)=115e6+hfs(n0)-2*zs(4);
                delta(2,12)=delta(2,8)+4*zs(4); delta(2,9)=115e6+lfs(n0)-zs(4);
                delta(2,10)=115e6+lfs(n0); delta(2,11)=delta(2,9)+2*zs(4);
                delta(3,1)=-129e6+hfs(n0); delta(3,2)=delta(3,1);
                delta(3,3)=delta(3,1); delta(3,4)=-74e6+hfs(n0);
                delta(3,5)=hfs(n0); delta(3,7)=delta(3,5);
                delta(3,6)=lfs(n0); delta(3,8)=41e6+hfs(n0);
                delta(3,12)=delta(3,8); delta(3,9)=41e6+lfs(n0);
                delta(3,10)=delta(3,9); delta(3,11)=delta(3,9);
                delta(4,1)=-170e6+hfs(n0); delta(4,2)=delta(4,1);
                delta(4,3)=delta(4,1); delta(4,4)=-115e6+hfs(n0);
                delta(4,5)=-41e6+hfs(n0); delta(4,7)=delta(2,5);
                delta(4,6)=-41e6+lfs(n0); delta(4,8)=hfs(n0);
                delta(4,12)=delta(4,8); delta(4,9)=lfs(n0);
                delta(4,10)=delta(4,9); delta(4,11)=delta(4,9);
                if L(n2)>0
                initial(1:12)=1/12;
                initial(13:17)=0;  %initial concentrations of ground
                                   %states 1:12, excited states 13:16 and
                                   %v">0 17
                ns=s(1,1)+s(1,2)+s(1,3)+s(1,4); %number of sidebands
                I=Intensity(n1)/ns; %define intensity per sideband
                range=[-L(n2)/2 L(n2)/2]; %define interaction zone
                [Z,P]=ode15s(@(z,N) SRF(z,N,I,delta,B,fc,gamma,Gamma,rmr,v,s),
                    range,initial);
                % UNCOMMENT: see the population dynamics (solution of MLRE)
                % make sure N1=N2=1 and define one Intensity and L point
                % of interest
                % HFS=P(:,1)+P(:,2)+P(:,3)+P(:,4)+P(:,5)+P(:,7)+P(:,8)+P(:,12)
                % LFS=P(:,6)+P(:,9)+P(:,10)+P(:,11)
                % ES=P(:,13)+P(:,14)+P(:,15)+P(:,16)
                % HVS=P(:,17)
                % plot(Z,HFS,'r',Z,LFS,'b',Z,HVS,'c',Z,ES,'k');
                gain_mol(n0)=(((P(end,6)+sum(P(end,(9:11))))-(1/3))/(1/3))*100;
                clear Z P
                else
                gain_mol(n0)=0;
                end
                clear delta
                end
        gain(n1,n2)=sum(sum(gain_mol))/size(lfs,2);
        end
end
```

```
%% plotting
set(gca,'FontSize',20);
contourf(L,Intensity,gain); xlabel('Interaction_length_(mm)');
ylabel('I/I_s'); title('Gain_in_LFS_molecules_(%)'); colorbar;
h=colorbar; set(h,'fontsize',20);
% UNCOMMENT: 2D plotting (optional)
% figure; set(gca,'FontSize',20);
% plot(Intensity,gain(:,1:N2)); xlabel('I/I_s');
%% data acquisition
% UNCOMMENT: save the parameter vectors and the gain matrix
name = ['data/gain_',num2str(N1),'_I_points_',num2str(N2),'_L_points_',num2str(
    sum(s)),'_sidebands_max_intensity_',num2str(max_intensity),'
    _max_interaction_length_',num2str(max_L),'_volt_',num2str(volt),'_distr_',
    num2str(distr),'_B_field_0.0005.mat']
save(name,'Intensity','L','gain')
```

Appendix E

'Stark_shift_distr_1_calculate_sp.m'

```
% This program calculates sample points for distribution 1.
% The input is the voltage 'volt' and number of sample points 'N'.
% The step '%% define the real trap' have to be done manually for each
% voltage magnitude. The boundary value's of the x and y axis from one of
% the subplots of figure(1), forming a closing trap have to be inserted in
% the 'if'-loop. The output are two vectors 'lfs' and 'hfs', each with 'N'
% random values for the lfs and hfs differential stark shift.
clear all; close all;
%% define parameters
volt=1; %define the voltage amplitude
grid=0.058824e-3 %define mm per grid point
N=10; %define number of molecules
%% load relevant files
name=['stark_shift_',num2str(volt),'_kV_distr_1.mat']
load(name);
%% calculate stark shift low-field seeking ground state
figure; subplot(2,2,1);
surf(STARK_lfs_gs(690:787,34:67)) %find out the size of one trap
ss(:,:,1)=STARK_lfs_gs(690:787,34:67)'.*100*2.998e8; %define one trap matrix
S=size(ss(:,:,1)); %calculate size
z=linspace(-((S(2)/2)-1)*grid,((S(2)/2)-1)*grid,S(2)); %define z vector
r=linspace(0,S(1)*grid,S(1)); %define r vector
ss(:,:,1)=ss(:,:,1)-min(min(ss(1:10,40:60,1))); %normalize for zero field
figure; subplot(2,2,1); contour(z,r,ss(:,:,1),50); %plot contour
xlabel('Longitudinal position z (mm)'); ylabel('Radial position r (mm)')
title('Stark Shift lfs gs (cm^{-1})'); colorbar;
%% calculate stark shift high-field seeking ground state
figure(1); subplot(2,2,2);
surf(STARK_hfs_gs(690:787,34:67)) %find out the size of one trap
ss(:,:,2)=STARK_hfs_gs(690:787,34:67)'.*100*2.998e8; %define one trap matrix
ss(:,:,2)=ss(:,:,2)-max(max(ss(1:10,40:60,2))); %normalize for zero field
figure(2); subplot(2,2,2); contour(z,r,ss(:,:,2),50); %plot contour
xlabel('Longitudinal position z (mm)'); ylabel('Radial position r (mm)')
title('Stark Shift hfs gs (cm^{-1})'); colorbar;
%% calculate stark shift low-field seeking excited state
figure(1); subplot(2,2,3);
surf(STARK_lfs_es(690:787,34:67)) %find out the size of one trap
ss(:,:,3)=STARK_lfs_es(690:787,34:67)'.*100*2.998e8; %define one trap matrix
ss(:,:,3)=ss(:,:,3)-min(min(ss(1:10,40:60,3))); %normalize for zero field
figure(2); subplot(2,2,3); contour(z,r,ss(:,:,3),50); %plot contour
xlabel('Longitudinal position z (mm)'); ylabel('Radial position r (mm)')
title('Stark Shift lfs es (cm^{-1})'); colorbar;
%% calculate stark shift high-field seeking excited state
figure(1); subplot(2,2,4);
surf(STARK_hfs_es(690:787,34:67)) %find out the size of one trap
ss(:,:,4)=STARK_hfs_es(690:787,34:67)'.*100*2.998e8; %define one trap matrix
ss(:,:,4)=ss(:,:,4)-max(max(ss(1:10,40:60,4))); %normalize for zero field
figure(2); subplot(2,2,4); contour(z,r,ss(:,:,4),50); %plot contour
xlabel('Longitudinal position z (mm)'); ylabel('Radial position r (mm)')
title('Stark Shift hfs es (cm^{-1})'); colorbar;
%% define the real trap
```

```
for n1=1:1:S(1)
    for n2=1:1:S(2)
        if n1>28 | n2<34 | n2>65
        ss(n1,n2,1)=0; ss(n1,n2,2)=0;
        ss(n1,n2,3)=0; ss(n1,n2,4)=0;
        end
    end
end
figure; subplot(2,2,1); surf(z,r,ss(:,:,1)); colorbar;
figure(3); subplot(2,2,2); surf(z,r,ss(:,:,2)); colorbar;
figure(3); subplot(2,2,3); surf(z,r,ss(:,:,3)); colorbar;
figure(3); subplot(2,2,4); surf(z,r,ss(:,:,4)); colorbar;
min(min(ss(1:10,40:60,1)))
max(max(ss(1:10,40:60,2)))
min(min(ss(1:10,40:60,3)))
max(max(ss(1:10,40:60,4)))
%% define stark shift of the molecules
ss=ss(1:28,34:65,:);
z_mol= 1+(size(ss,2)-1)*rand(N); r_mol=1+(size(ss,1)-1)*rand(N);
for n=1:1:4
sp(:,:,n)=interp2(ss(:,:,n),z_mol,r_mol);
dummy(n,:) = reshape(sp(:,:,n),1,size(sp,1)*size(sp,2));
end
%% lfs (hfs) is differential stark shift between lfs es and lfs (hfs) gs
hfs=dummy(3,:)-dummy(2,:); lfs=(dummy(3,:)-dummy(1,:));
name=['stark_shift_',num2str(volt),'_kV_distr_1_sp.mat']
save(name,'lfs','hfs')
```